© 2014. Published by The Company of Biologists Ltd | Development (2014) 141, 3050-3061 doi:10.1242/dev.107680

RESEARCH ARTICLE

Hand1 phosphoregulation within the distal arch neural crest is essential for craniofacial morphogenesis

Beth A. Firulli[1], Robyn K. Fuchs[2], Joshua W. Vincentz[1], David E. Clouthier[3] and Anthony B. Firulli[1,*]

ABSTRACT

In this study we examine the consequences of altering Hand1 phosphoregulation in the developing neural crest cells (NCCs) of mice. Whereas *Hand1* deletion in NCCs reveals a nonessential role for Hand1 in craniofacial development and embryonic survival, altering Hand1 phosphoregulation, and consequently Hand1 dimerization affinities, in NCCs results in severe mid-facial clefting and neonatal death. *Hand1* phosphorylation mutants exhibit a non-cell-autonomous increase in pharyngeal arch cell death accompanied by alterations in *Fgf8* and *Shh* pathway expression. Together, our data indicate that the extreme distal pharyngeal arch expression domain of Hand1 defines a novel bHLH-dependent activity, and that disruption of established Hand1 dimer phosphoregulation within this domain disrupts normal craniofacial patterning.

KEY WORDS: Hand1, bHLH, Craniofacial development, Transcription, Dimerization, Phosphorylation, Neural crest

INTRODUCTION

Neural crest cells (NCCs) are a multipotent cell population that specifies within the dorsal lip of the neural tube and subsequently delaminates, migrates and populates the pharyngeal arches (PAs), before ultimately differentiating into a wide spectrum of structures/tissues along the anterior-posterior (AP) axis of vertebrate embryos (Clouthier et al., 2010; Minoux and Rijli, 2010; Ruest and Clouthier, 2009; Trainor, 2005; Gitton et al., 2010). The NCCs that migrate into the first and second PAs are primarily responsible for orchestrating craniofacial development. Well-integrated signaling programs function through transcription factors to define tissue patterning and NCC differentiation. The complex signals that govern craniofacial morphogenesis involve a number of input pathways, including Fgf, Shh, Wnt, Bmp, Pdgf, retinoic acid (RA) and endothelin signaling (Abe et al., 2008; Abzhanov and Tabin, 2004; Clouthier et al., 2003; Jiang et al., 2006; Kurihara et al., 1995; Macatee et al., 2003). Dysregulation of NCC migration, proliferation and patterning can result in craniofacial abnormalities observed in numerous human syndromes (Chai and Maxson, 2006; Jiang et al., 2006; Noden and Trainor, 2005; Clouthier et al., 2013). Indeed, cleft lips and cleft palates are among the most common congenital defects observed in newborns. Understanding the signaling pathways and downstream transcription factors that govern craniofacial morphogenesis is crucial in defining the etiology of these common congenital defects.

Members of the basic helix-loop-helix (bHLH) transcription factor superfamily play dominant roles in cell specification, differentiation and tissue patterning throughout embryonic development (Massari and Murre, 2000). bHLH transcription factors affect transcription by forming either a bHLH homo- or heterodimer and by binding DNA via a *cis*-element termed E-box. Loss-of-function studies in the Twist sub-class of bHLH factors, which include Twist1, Twist2, Hand1 and Hand2 (Barnes and Firulli, 2009), reveal that these factors play key roles in craniofacial morphogenesis. Targeted disruption of *Twist1* in NCCs leads to defects in upper and lower jaw development (Bildsoe et al., 2009). NCC-specific deletion of *Hand2* results in disruption of lower jaw and tongue development (Barron et al., 2011). These factors appear highly conserved during vertebrate evolution (Barnes and Firulli, 2009) and probably play similar roles in human facial development. Indeed, human mutations in *TWIST1* cause Saethre–Chotzen syndrome (SCS). In addition to craniosynostosis, palatal anomalies are commonly observed in SCS patients (Stoler et al., 2009).

Compelling evidence shows that Twist family bHLH factors mediate biological function by dimer choice (Castanon et al., 2001; Firulli et al., 2003, 2005, 2007). Dimer choice is regulated, in part, by a threonine and serine pair that is evolutionarily conserved among all Twist family members. Mimicking Hand1 hypophosphorylation through mutations in residues T107 and S109 enhances homodimer formation, whereas mimicking Hand1 phosphorylation at T107 and S109 enhances formation of E-protein heterodimers (Firulli et al., 2003). Indeed, changes in bHLH dimer choices affect craniofacial development (Connerney et al., 2006). Dysregulation of Twist1 phosphorylation at these threonine and serine residues causes SCS (Cai and Jabs, 2005; Firulli et al., 2005). Dimerization of Twist-family bHLH factors is governed by their co-expression within a cell, their colocalization within the nucleus, their level of relative expression and the phosphorylation of the conserved threonine and serine residues within Helix I of the bHLH domain (Firulli and Conway, 2008; Firulli et al., 2003, 2005, 2007). Overexpression studies alter the stoichiometry of this bHLH pool. Thus, to validate the consequences of dysregulating this post-translational control mechanism within the bHLH dimer pool *in vivo*, it is essential to manipulate phosphorylation but not expression levels.

By contrast to the dominant roles exhibited by Twist1 and Hand2 in craniofacial development, the related factor Hand1, although expressed within the distal most NCC-derived PA mesenchyme (Clouthier et al., 2000), shows no observable phenotypes in NCC loss-of-function analysis. However, there is a clear gene dosage effect when *Hand1* NCC conditional-null mice are placed on a *Hand2* heterozygous background (Barbosa et al., 2007). This suggests a crucial *Hand* gene dosage that, when disrupted, perturbs the bHLH dimer pool within cranial NCCs, resulting in morphogenic defects. To test whether Hand1 phosphorylation-dependent dimer regulation

[1]Riley Heart Research Center, Herman B Wells Center for Pediatric Research, Division of Pediatric Cardiology, Departments of Anatomy and Medical, Biochemistry, and Molecular Genetics, Indiana Medical School, 1044 W. Walnut Street, Indianapolis, IN 46202-5225, USA. [2]Department of Physical Therapy and the Center for Translational Musculoskeletal Research, School of Health and Rehabilitation Science, Indiana University, Indianapolis, IN 46202, USA. [3]Department of Craniofacial Biology, University of Colorado Anschutz Medical Campus, 12801 E 17th Avenue, Rm. 11-109, MS 8120, Aurora, CO 80045, USA.

*Author for correspondence (tfirulli@iupui.edu)

Received 30 December 2013; Accepted 29 May 2014

Development (2014) 141, 3050-3061 doi:10.1242/dev.107680

alters the composition of the bHLH dimer pool, which influences craniofacial morphogenesis, we engineered two *Hand1* conditional-activation knock-in alleles designed to either mimic Hand1 hypophosphorylation by replacing both threonine 107 and serine 109 with alanines (PO_4−), or to mimic Hand1 hyperphosphorylation by replacing these residues with aspartic acids (PO_4+). Activation of these phospho-mutant alleles within NCCs results in severe mid-facial clefting. Mutant embryos display abnormal cell death within the developing PAs, resulting in reduced outgrowth of the maxillary processes and aberrant craniofacial development. The majority of structural defects occur within tissues where *Hand1* is not expressed and where *Hand1*-lineage cells are not detected. Gene expression analyses show that both fibroblast growth factor 8 (Fgf8) and sonic hedgehog (Shh) signaling pathways are affected. Interestingly, removing the wild-type *Hand1* allele on both the $Hand1^{PO4-}$ and $Hand1^{PO4+}$ backgrounds results in reduced levels of cell death and improved craniofacial development. Together, these results show that, although Hand1 is dispensable for development of craniofacial structures, a misregulation of Hand1 dimer choice within the NCC-derived distal PA ectomesenchyme disrupts the function of other factors required for craniofacial morphogenesis. These findings suggest that Hand1 and its putative bHLH dimer partners transcriptionally control one or more of the theorized cap signals central to the 'Hinge and Caps' model of PA patterning (Depew and Compagnucci, 2008; Fish et al., 2011).

RESULTS

Hand1 phospho-mutant expression within the PAs results in pronounced mid-facial clefts

To understand the role of Hand1 phosphoregulation within NCCs, we engineered two targeted conditionally active *Hand1* alleles, wherein residues T107 and S109 were replaced with either alanines (PO_4−) or aspartic acids (PO_4+; Fig. 1A). By incorporating a Stop-flox cassette containing a neomycin resistance gene downstream of the *Hand1* transcriptional start site, but upstream of the Hand1-initiating methionine, we were able to create null, conditional phospho-mutant *Hand1* alleles. In tissues where the *Cre* recombinase and endogenous *Hand1* expression directly overlap, the Stop-flox cassette is removed, allowing expression of the $Hand1^{PO4-}$ or $Hand1^{PO4+}$ mutant alleles. *Hand1* expression within NCC-derived mesenchyme of the distal PAs is first detectable at E9.5. Expression cannot be detected at E9.0 using the sensitive $Hand1^{lacZ}$ knock-in allele (Firulli et al., 1998; Fig. 1B-E). *Hand1* expression initiates in the most posterior/caudal portions of the distal PA before expanding anteriorly/rostrally, but not laterally. At E13.5, *Hand1*-expressing cells mark the medial tongue (t) and fusion point of the two mandibular halves (md; Fig. 1F,G). Although *Hand1*-lineage analysis reveals minor lateral spreading of these distal cells, *Hand1* expression is lost as the cells move laterally from the midline. Craniofacial structures of the calvarium do not express *Hand1* or contain *Hand1* lineage cells (Barnes et al., 2010).

We tested the efficacy of our conditional *Hand1* phospho-mutant alleles by activating mutant expression in NCCs using the *Wnt1-Cre* allele (Danielian et al., 1998). Whole-mount *in situ* hybridization (ISH) of *Hand1* detects distal expression in the forming PAs of control embryos (Fig. 1H-J). To demonstrate that the conditional alleles show the expected *Hand1* spatio-temporal pattern, we crossed both the $Hand1^{PO4-}$ and $Hand1^{PO4+}$ mutant alleles onto the *Hand1* conditional ($Hand1^{fx}$) allele (Barbosa et al., 2007; McFadden et al., 2005), and then recombined both conditional alleles in NCCs using the *Wnt1-Cre* allele. Using $Hand1^{PO4-/fx}$;*Wnt1-Cre(+)* and $Hand1^{PO4+/fx}$;*Wnt1-Cre(+)* embryos, we demonstrate that mRNA expression from either of the *Hand1* phospho-mutant alleles is indistinguishable from wild-type *Hand1* or the $Hand1^{lacZ}$ expression by *Hand1* ISH (Fig. 1I,J). However, *Wnt1-Cre*-mediated expression of both *Hand1* phospho-mutant alleles results in neonatal death accompanied by 100% penetrant mid-face clefts (Fig. 1L-N).

To determine when we could first detect a facial phenotype, we collected mutant embryos from timed pregnancies between E10.5 and E19.5. $Hand1^{+/PO4-}$;*Wnt1-Cre(+)*, $Hand1^{+/PO4+}$;*Wnt1-Cre(+)*, $Hand1^{PO4-/fx}$;*Wnt1-Cre(+)* and $Hand1^{PO4+/fx}$;*Wnt1-Cre(+)* phenotypes are first morphologically identifiable at E10.5, wherein distances between the lateral nasal prominences (lnp) and the olfactory pits (op, black line) are extended and maxillary processes (mp) are symmetrically reduced in size (supplementary material Fig. S1). As development proceeds, the extent of this phenotype becomes more evident. Surprisingly, removal of the wild-type *Hand1* allele reduces the severity of both hypophosphorylated and phosphorylation-mimicking phenotypes. Histological analysis at E14.5 shows that structures such as tooth primordia (tp), Meckel's cartilage (mc) and nasal cavities (nc) form normally in the *Hand1* phospho-mutant embryos (supplementary material Fig. S2). The nasal capsule is also present but is deviated down the midline with the rest of the facial structures. By contrast, *Hand1* phospho-mutant heterozygotes [$Hand1^{+/PO4-}$;*Wnt1-Cre(+)* and $Hand1^{+/PO4+}$;*Wnt1-Cre(+)*] lack a patent nasal septum (does not fuse at the midline; ns; black asterisk; supplementary material Fig. S2G,I). Furthermore, the palatal shelves (ps) are not fused, resulting in aberrant communication between the nasopharynx and oral cavity (supplementary material Fig. S2B,D). Single-copy point mutants [$Hand1^{PO4-/fx}$;*Wnt1-Cre(+)* and $Hand1^{PO4+/fx}$;*Wnt1-Cre(+)*] show improvement in nasal septum development (supplementary material Fig. S2H,J), and in the case of $Hand1^{PO4+/fx}$;*Wnt1-Cre(+)* embryos, palatal shelf fusion is observed in mixed penetrance, although clefting is still fully penetrant (supplementary material Fig. S2E,J).

We next employed micro-computed tomography (micro-CT) scans of heads from P0 $Hand1^{+/PO4-}$;*Wnt1-Cre(+)*, $Hand1^{+/PO4+}$;*Wnt1-Cre(+)*, $Hand1^{PO4-/fx}$;*Wnt1-Cre(+)* and $Hand1^{PO4+/fx}$;*Wnt1-Cre(+)* embryos. In $Hand1^{PO4-/+}$ mutant embryos, structural defects were observed throughout the skull. On lateral view, the premaxilla (pm, dark purple) is shortened, and both the overlying nasal bone (n, green) and a portion of the maxilla (mx, blue) closest to the frontal bone (f, red) are missing (Fig. 1L). The jugal bone (j, dark red), the middle bone of the zygomatic arch (with the others being the zygomatic processes of the maxilla and squamosal bones), is hypoplastic, and the squamosal bone (sq, light purple) is absent (Fig. 1K). The proximal mandible (md, bronze) is also hypoplastic. In dorsal view (Fig. 1L), the interparietal (i, turquoise) and frontal bones are hypoplastic, the latter leading to a large gap between the frontal bones. The upper incisors (magenta, white arrow) are readily visible due to this hypoplasia and the absence of the nasal bone. Both sagittal sutures are also aberrantly fused (asterisk). The hypoplasia of the mandible is more obvious from the dorsal view, with the two halves failing to meet at the midline. A ventral view (Fig. 1M) reveals more significant changes to the skull base. Whereas the midline defects around the premaxilla are obvious, most bones appear hypoplastic. The basisphenoid (bs, uncolored) and pterygoid bones (pt, uncolored) are severely underdeveloped, with the missing squamosal bone more obvious. Also missing is the lamina obturans (the bony portion of the future alisphenoid that abuts the squamosal bone). In addition, the midline cleft defect resulted in the failure of the palatine bones and the palatal processes of the maxilla to fuse (pl, yellow). To examine cartilage derivatives, we stained E17.0 control and $Hand1^{+/PO4+}$;

Development (2014) 141, 3050-3061 doi:10.1242/dev.107680

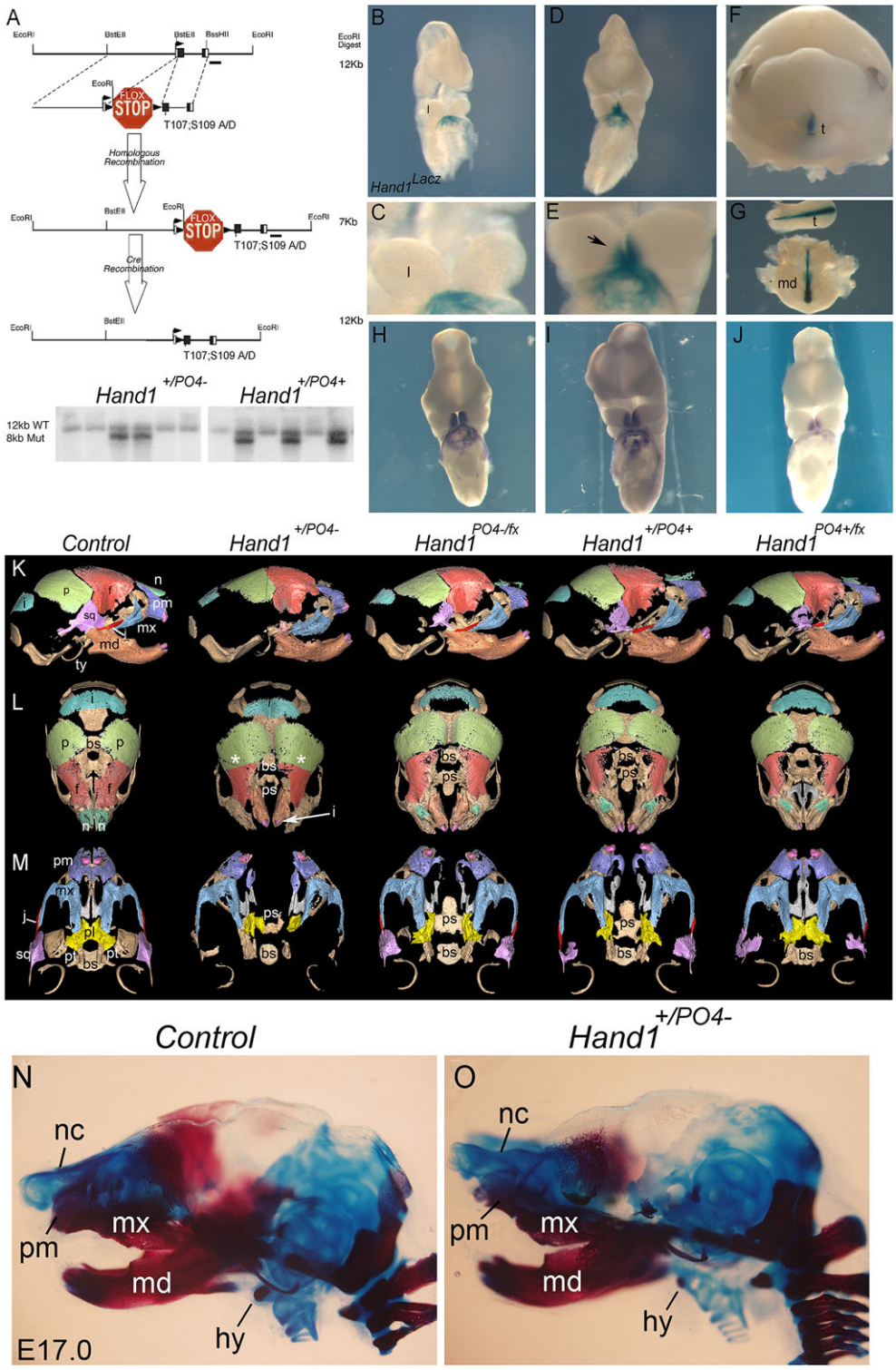

Fig. 1. Expression and craniofacial phenotypes of *Hand1* phospho-mutant mice. (A) Targeting design and Southern blot restriction fragment length polymorphism (RFLP) analysis of the *Hand1*$^{PO4-}$ and *Hand1*$^{PO4+}$ mutant alleles. (B-G) β-galactosidase staining of *Hand1*^{lacZ} embryos (hearts removed prior to staining) at E9.0 (B,C), E9.5 (D,E) and E13.5 (F,G) showing the distal expression of *Hand1* initiating within the first arch (marked in B,C as 'l') between E9.0 and E9.5 (black arrow in E). Expression is limited to the most distal arch tissue, which at E13.5 marks the central tongue (t) and mandible (md). (H-J) Whole-mount ISH showing *Hand1* expression within the medical arch mesenchyme in wild type (H) and in *Hand1*$^{PO4-/fx}$ (I) and *Hand1*$^{PO4+/fx}$ (J) single copy mutants (hearts removed prior to hybridization). (K-M) Micro-CT images of P0 skulls from control, *Hand1*$^{+/PO4-}$, *Hand1*$^{PO4-/fx}$, *Hand1*$^{+/PO4+}$ and *Hand1*$^{PO4+/fx}$ embryos shown from the right lateral (K), dorsal (L) and ventral (M) sides of the skulls. Abbreviations for row K: i, interparietal bone (turquois); p, parietal bone (light green); f, frontal bone (red); n, nasal bone (green); sq, squamosal bone (light purple); pm, premaxilla (dark purple); j, jugal bone (dark red); mx, maxilla (blue); md, mandible (bronze); ty, tympanic bone (uncolored). Abbreviation for row L: i, incisors (magenta, indicated by white arrow). Abbreviations for row M: pl, palatine bones (yellow); bs, basisphenoid (uncolored); pt, pterygoid bones (uncolored). $n \geq 4$ for each genotype. Bone and cartilage staining of control (N) and *Hand1*$^{+/PO4-}$ mutant (O). Maxilla, (mx); hyoid (hy).

Development (2014) 141, 3050-3061 doi:10.1242/dev.107680

Wnt1-Cre(+) embryos with alizarin red and alcian blue to visualize bone and cartilage, respectively. Compared with control embryos (Fig. 1N), the malleus and incus (mandibular arch) as well as the stapes (second PA) appear normal in *Hand1*$^{+/PO4+}$;*Wnt1-Cre(+)* embryos (Fig. 1O). However, Meckel's cartilage (mandibular arch) is truncated at its origin with the malleus, and the cartilage anlage of the hyoid bone (second arch) is poorly ossified and deformed at the midline.

Defects in *Hand1*$^{PO4-/fx}$;*Wnt1-Cre(+)* embryos, in which only the mutant *Hand1* allele is present, are less severe. In lateral view (Fig. 1K), the squamosal, jugal and tympanic ringbones appear normal, as does the premaxilla and the mandible. The nasal bone is present but hypoplastic. In dorsal view (Fig. 1L), the midline defects in the front bones are apparent, as hypoplasia of the nasal bone allows visualization of the upper incisors. The sagittal sutures appear normal. In ventral view (Fig. 1M), there is modest improvement in the pterygoid bones, although the basisphenoid is still hypoplastic. The size of the lamina obturans and squamosal bones are also improved compared with *Hand1*$^{+/PO4-}$ embryos. The trabecular basal plate is also better developed, although there is still a significant cleft between the palatal processes of the palatine and maxilla bones and between the two halves of the premaxilla.

In *Hand1*$^{+/PO4+}$;*Wnt1-Cre(+)* embryos, a lateral view shows that the premaxilla, nasal, and the squamosal bones are better formed, but are still slightly hypoplastic. The proximal mandible also appears slightly smaller. In dorsal view, the distal mandible appears fused at the midline and the sagittal sutures appear normal. By contrast, the midline cleft in the maxilla appears more severe than observed in *Hand1*$^{+/PO4-}$ mutants, with the defect extending into the parietal bones. The gap between the upper incisors is noticeably enlarged. Ventral changes in *Hand1*$^{+/PO4+}$ mutants are nearly identical to those observed in *Hand1*$^{+/PO4-}$ mutants. One additional difference is the absence of at least a portion of the ala temporalis portion of the alisphenoid.

In lateral view, *Hand1*$^{PO4+/fx}$;*Wnt1-Cre(+)* mutants appear nearly identical to *Hand1*$^{+/PO+}$;*Wnt1-Cre(+)* mutants, although the proximal mandible is slightly hypoplastic, as is the squamosal bone. On dorsal view, phenotypes are similar to *Hand1*$^{+/PO4+}$ mutants. On ventral view, the middle-ear ossicles are either hypoplastic or absent, although portions of the alisphenoid appear better developed. Interestingly, the palatal processes of the palatine and maxilla appear to fuse normally along the midline, although both structures are smaller than those in control embryos. The ectopic bone observed in *Hand1*$^{PO4+/fx}$;*Wnt1-Cre(+)* mutants is not present in *Hand1*$^{+/PO+}$;*Wnt1-Cre(+)* embryos. A detailed measure of bone sizes is shown in supplementary material Table S1.

Hand1 phospho-mutants exhibit increased cell death within the PAs

We postulated that the midline defects in facial structures could be the result of a defect in cell migration, the inability of the structures to fuse, decreased cell proliferation or increased cell death within the cranial NCC. We looked at NCC migration by utilizing *ROSA26*^{lacZ} reporter lineage-tracing and observed no obvious migration defects for the NCCs entering the PAs or cardiac outflow tract (supplementary material Fig. S3). Defects in tissue fusion seem unlikely, as fusion is observed in the *Hand1*$^{PO+/fx}$;*Wnt1-Cre(+)* mutants (Fig. 1; supplementary material Fig. S2), and the assessment of the fusion markers *Jagged2* and *Mmp13* reveal no significant variations between E14.5 control and *Hand1*$^{+/PO4-}$;*Wnt1-Cre(+)* or *Hand1*$^{+/PO4+}$;*Wnt1-Cre(+)* embryos (supplementary material Fig. S4). 5-Ethynyl-2′-deoxyuridine (EdU) incorporation analysis reveals no significant difference in NCC proliferation between control and all *Hand1* phospho-mutant embryos at E9.5 and E10.5 (data not shown). By contrast, significantly elevated levels of cell death are observed within the PAs of *Hand1* phospho-mutant embryos compared with control littermates (Fig. 2). At E9.5, whole-mount LysoTracker staining of control embryos reveals two dorsally localized domains of normal developmental cell death (black arrows) with low levels of cell death detected within the PA mesenchyme (Fig. 2A, white arrow). This is confirmed by section terminal deoxynucleotidyl transferase dUTP nick end labeling (TUNEL) analysis (Fig. 2C, yellow arrows indicating developmental cell death). E9.5 *Hand1*$^{+/PO4-}$;*Wnt1-Cre(+)* mutant embryos exhibit a marked reduction in the developmental dorso-lateral cell death domains while displaying a marked increase in PA cell death as assayed by both LysoTracker and TUNEL staining (Fig. 2E,G). Correlating with the less severe clefting phenotype, *Hand1*$^{PO4-/fx}$;*Wnt1-Cre(+)* mutants display levels of normal dorso-lateral developmental cell death similar to controls, while at the same time exhibiting decreased cell death within the PA mesenchyme (Fig. 2I,K). Similar findings are observed in *Hand1*$^{PO+/fx}$;*Wnt1-Cre(+)* embryos (Fig. 2M,O). At E10.5, the extent of cell death within the PA of the phospho-mutants is reduced when compared with control embryos (Fig. 2B,D,F,H,J,L,N,P,R,T). Given that the *Hand1* expression domain (Fig. 1) does not directly overlap with the observed domain of PA cell death, we reasoned that a cell signaling pathway is disrupted in *Hand1* phospho-mutant embryos and that the observed craniofacial phenotypes are generated non-cell autonomously.

Hand1 phospho-mutants show alterations in signaling pathways that regulate craniofacial formation

During craniofacial formation, numerous signaling pathways intersect to govern normal morphological patterning and include Fgf, Shh, Wnt, Bmp and RA signaling (Clouthier et al., 2010; Trainor, 2005). We first looked at altered RA signaling as *Rdh10* mutant mice exhibit similar mid-facial clefting (Sandell et al., 2007). By intercrossing *Hand1* phospho-mutant mice with the *RARE-lacZ* reporter line (Rossant et al., 1991), we found that *RARE-lacZ* patterning was largely unaffected in both *Hand1*$^{+/PO4-}$;*RARE-lacZ(+)*;*Wnt1-Cre(+)* and *Hand1*$^{+/PO4+}$;*RARE-lacZ(+)*;*Wnt1-Cre(+)* embryos at E10.5 and E11.5 (supplementary material Fig. S5). Likewise, expression of both *Bmp2* and *Bmp4* shows no appreciable difference between mutant and control embryos (data not shown).

We next examined *Fgf8* expression in control and *Hand1* mutant embryos between E9.5 and E12.5 (Fig. 3). Mouse models that exhibit variation in *Fgf8* gene dosage and *Fgf8* gain-of-function studies in chicks both present with mid-face clefts that are accompanied by early cell death (Abzhanov and Tabin, 2004; Chen et al., 2012; Griffin et al., 2013; Moon and Capecchi, 2000). *Fgf8* expression between E9.5 and 12.5 shows a marked expansion in *Hand1* phospho-mutants when compared with control embryos. *Fgf8* expression within the rostral portion of the first arch, the maxillary processes and surrounding the nasal pits is expanded and becomes more pronounced over time (Fig. 3: compare D with H, L, P and T). Levels of *Fgf8* expression appear more persistent in E12.5 mutant embryos where olfactory pit expression is more robust and expression at the edge of the maxilla is still visible (Fig. 3D,H,L,P,T, white arrows).

To validate this observation, we next looked at the expression of sprouty homolog 1 (*Spry1*) and ets variant 5 (*Etv5*), both downstream mediators of Fgf8/*FgfR1* signaling (Firnberg and Neubüser, 2002; Lunn et al., 2007; Minowada et al., 1999; Raible and Brand, 2001), in *Hand1*$^{+/PO4-}$;*Wnt1-Cre(+)* and *Hand1*$^{+/PO4+}$;*Wnt1-Cre(+)* embryos at E10.5 (Fig. 4). Similar to *Fgf8* expression, *Spry1* expression is expanded around the first PA and surrounding the olfactory pits in both *Hand1*$^{+/PO4-}$;*Wnt1-Cre(+)* and *Hand1*$^{+/PO4+}$;*Wnt1-Cre(+)* mutants

Development (2014) 141, 3050-3061 doi:10.1242/dev.107680

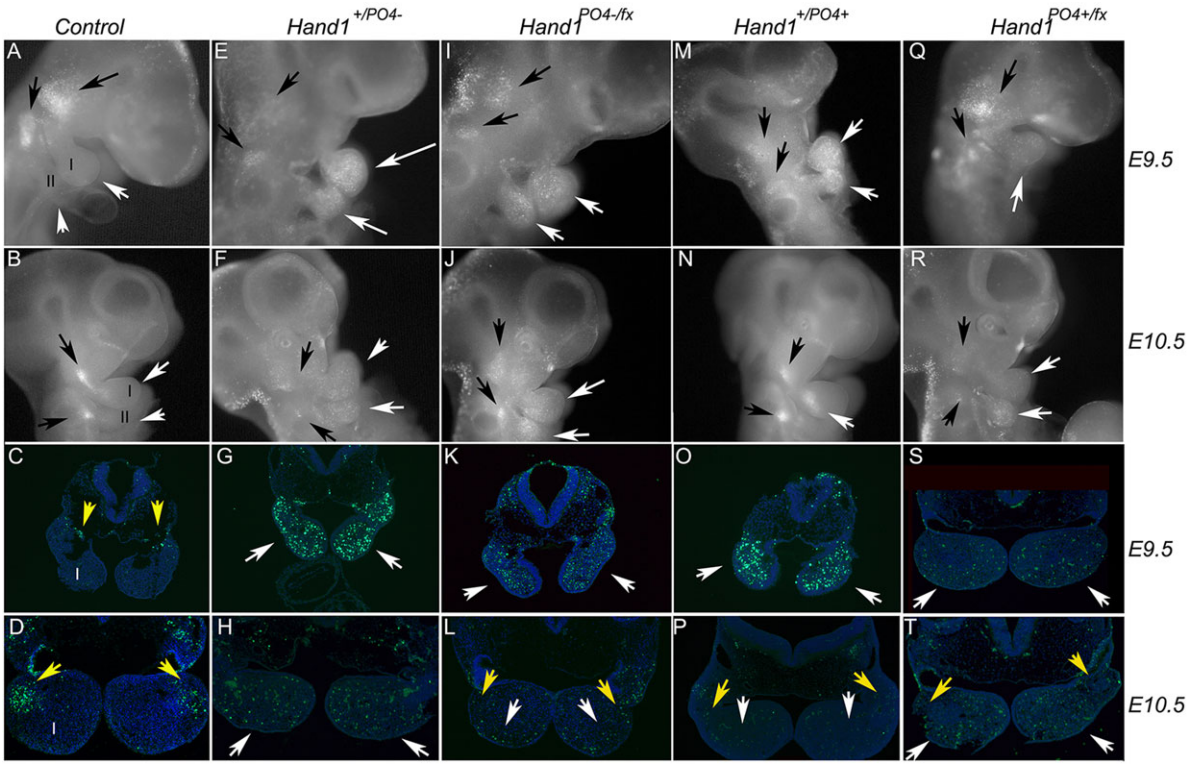

Fig. 2. Cell death analysis in *Hand1* phospho-mutant embryos. Control (A-D), $Hand1^{+/PO4-}$ (E-H), $Hand1^{PO4-/fx}$ (I-L), $Hand1^{+/PO4+}$ (M-P) and $Hand1^{PO4+/fx}$ (Q-T) were assayed for cell death using LysoTracker (whole mounts) and TUNEL (sections) at E9.5 and E10.5. Black arrows in whole mount and yellow arrows in sections mark developmental cell death observed in all controls, white arrows indicate cell death within the PAs that is increased in *Hand1* phospho-mutants. I, first pharyngeal arch; II, second pharyngeal arch. $n \geq 4$ for each genotype.

when compared with control littermates (Fig. 4B,C, asterisks). Expression of *Etv5* is also expanded. In control embryos, *Etv5* mRNA is observed to be more robust within the rostral portion of the first PA (Fig. 4D, black arrow). In comparison, *Etv5* expression within the first PA of both the $Hand1^{+/PO4-}$ and $Hand1^{+/PO4+}$ phospho-mutant embryos shows a clear caudal expansion (Fig. 4E,F, white arrows). The expression of the *FgfR1* shows no significant differences in expression patterns (Fig. 4G-I). We next performed qRT-PCR on

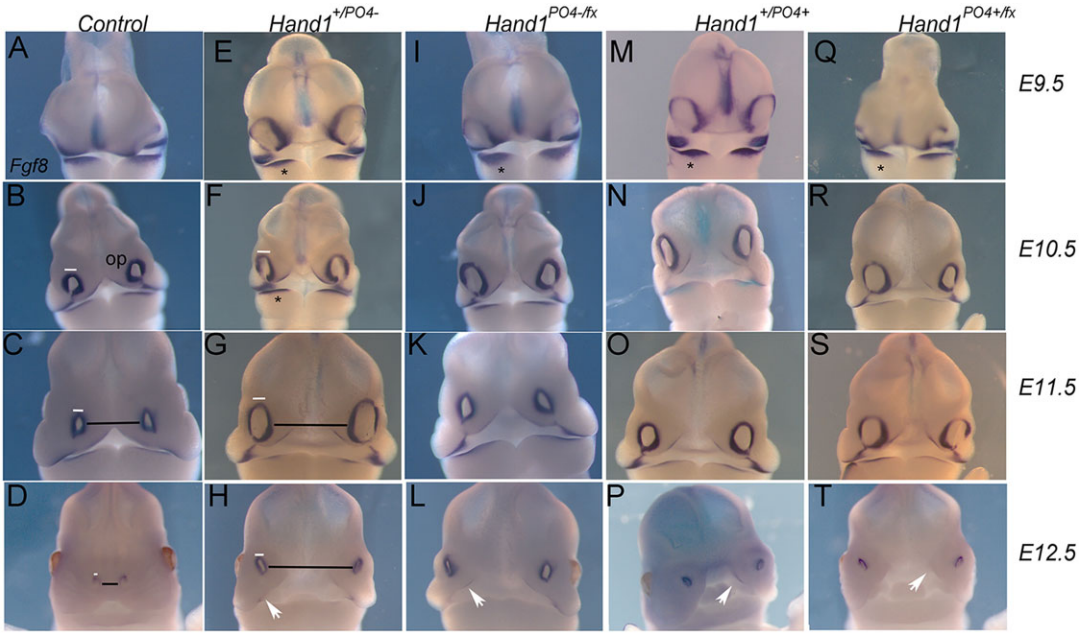

Fig. 3. *Fgf8* craniofacial expression in *Hand1* phospho-mutant embryos. Control (A-D), $Hand1^{+/PO4-}$ (E-H), $Hand1^{PO4-/fx}$ (I-L), $Hand1^{+/PO4+}$ (M-P) and $Hand1^{PO4+/fx}$ (Q-T) were assayed for *Fgf8* expression by whole-mount ISH. Asterisks show enhanced arch expression at E9.5. White bars in B-D,F-H show size differences in the diameter of the olfactory pits, and black bars in C,D,G,H show differences in distance between the olfactory pits of control and $Hand1^{+/PO4-}$ mutants. $n \geq 4$ for each genotype. White arrows in the bottom row indicate persistent *Fgf8* expression.

Development (2014) 141, 3050-3061 doi:10.1242/dev.107680

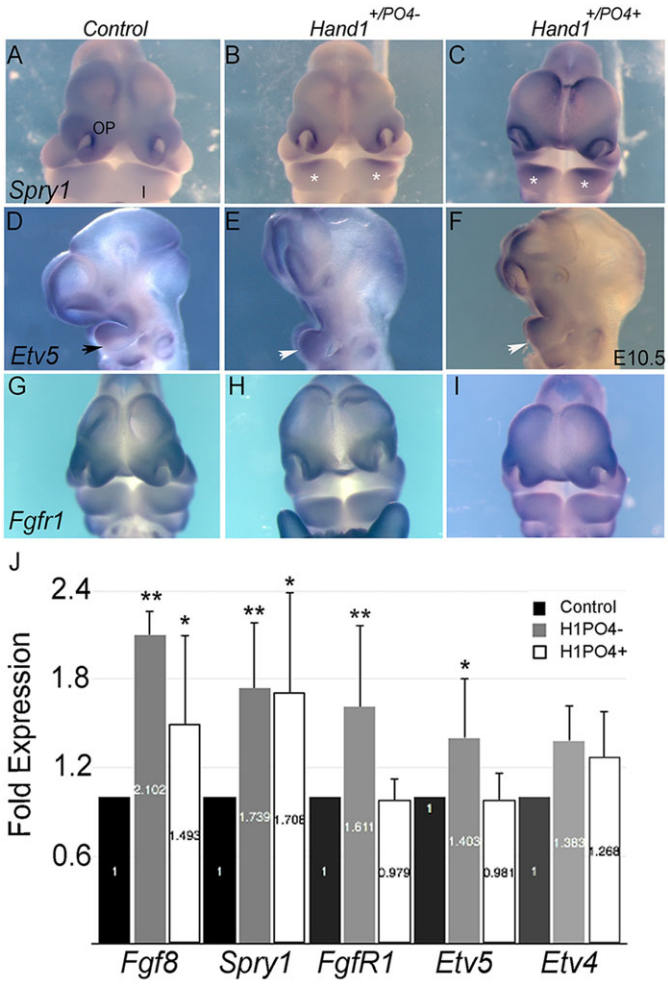

Fig. 4. Expression of *Fgf8* downstream responders *Spry1* and *Etv5* at E10.5. (A-I) *Hand1* phospho-mutant embryos and the Fgf8 receptor *FgfR1*. Control (A,D,G), *Hand1*$^{+/PO4-}$ (B,E,H) and *Hand1*$^{+/PO4+}$ (C,F,I) were assayed for *Spry1* (A-C), *Etv5* (D-F) and *FgfR1* (G-H) by whole-mount ISH. White asterisks denote enhanced *Spry1* expression within the first mandibular arches of *Hand1* phospho-mutants. Black arrowhead in D shows the more robust rostral versus caudal *Etv5* expression within the first mandibular arch. White arrowheads in E and F show caudal expansion of expression in both *Hand1*$^{+/PO4-}$ and *Hand1*$^{+/PO4+}$ phospho-mutants. I, first pharyngeal arch; op, olfactory pit. (J) Comparison of *FgfR1* expression between controls and phospho-mutants. qRT-PCR analysis of *Fgf8*, *Spry1*, *FgfR1*, *Etv5*, *Etv4*. Error bars denote s.e.m.; *P≤0.05 and **P≤0.01 by Student's *t*-test. n≥4 for each genotype.

cDNA reverse transcribed from RNA isolated from E10.5 control and *Hand1* point mutant heads (Fig. 4J). Results confirm qualitative observations, showing that *Fgf8*, *Spry1* and *Etv5* are significantly upregulated (*P≤0.05; **P≤0.01 n≥4) in both *Hand1*$^{+/PO4-}$ and *Hand1*$^{+/PO4+}$ phospho-mutant embryos when compared with controls. Interestingly, both *Etv5* and *FgfR1* expression are elevated in *Hand1*$^{+/PO4-}$ mutants but not in *Hand1*$^{+/PO4+}$ mutant embryos, and we observe no significant difference in *Etv4* expression (Fig. 4J).

In light of the expanded *Fgf8* expression, we next examined Shh signaling in *Hand1* phospho-mutant embryos. Shh is known to act synergistically with Fgf8 to drive cartilage outgrowth and cranial formation (Abzhanov and Tabin, 2004). Moreover, expanded Shh signaling is associated with a widening of the head (Abzhanov et al., 2007; Brugmann et al., 2006; Cobourne et al., 2009; Hu et al., 2003; Huang et al., 2007; Jeong et al., 2004; Jiang et al., 2006; Lan and Jiang, 2009). *Hand1* phospho-mutants exhibit a similar head expansion between the nasal pits (supplementary material Fig. S1). At E9.5, expanded expression of *Shh* is observed within *Hand1* phospho-mutant embryos when compared with controls (Fig. 5A-E, white asterisks). E11.5 control embryos (Fig. 5F) show undetectable *Shh* expression within the medial head ectoderm of the sinus cavity region, although robust expression is observed in the tooth primordia. By contrast, *Shh* expression is persistent in the sinus cavity of *Hand1* phospho-mutant embryos (Fig. 5G-K, white arrows) in addition to the tooth primordia (tp). Persistent *Shh* medial head ectoderm expression is observed up to E12.5 (Fig. 5K-O), with removal of the *Hand1* wild-type allele reducing the observed persistent expression. Additionally, strong *Shh* E12.5 expression is observed within the forming tooth primordia, rugae (r) and mystacial vibrissae (mv).

We next looked at the expression of patched 1 (*Ptch1*) in E9.5 embryos (Fig. 6A-C). When compared with control embryos, *Ptch1* expression appears unchanged in the forming head mesenchyme and first arch (black asterisk) of both *Hand1*$^{+/PO4-}$;*Wnt1-Cre(+)* and *Hand1*$^{+/PO4+}$;*Wnt1-Cre(+)* embryos. Enhanced PA expression (black asterisk) of the Shh-regulated transcription factor *Gli1* is observed in *Hand1* heterozygous phospho-mutants; however, no significant changes are observed in the expression of *Gli3* (Fig. 6D-I). To confirm these observations, we performed qRT-PCR on *Hand1*$^{+/PO4-}$; *Wnt1-Cre(+)* and *Hand1*$^{+/PO4+}$;*Wnt1-Cre(+)* phospho-mutant head cDNA (Fig. 6J). Results confirm that both *Shh* and *Gli1* expression are significantly enhanced in both *Hand1* phospho-mutants; however, *Ptch1* and *Gli3* expression levels are not significantly affected. Collectively, these data demonstrate non-cell-autonomous changes in both Fgf8 and Shh signaling pathways in *Hand1* phospho-mutant embryos.

Expression of *Twist1* is altered in *Hand1* phospho-mutant embryos

As Twist1 is a known integrator of Fgf and Shh signaling (Hornik et al., 2004), we next investigated the expression of *Twist1* in control and *Hand1* phospho-mutant embryos (Fig. 7). *Twist1* loss-of-function mutations are associated with craniofacial defects during embryogenesis (Chen and Behringer, 1995) and the disease SCS (Barnes and Firulli, 2009; Firulli et al., 2005; Jabs, 2004). At E10.5, *Twist1* is robustly expressed within the NCC of the medial and lateral nasal processes (lnp), the maxillary process (mp), as well as the first (I) and second (II) PAs (Fig. 7A). In E10.5 *Hand1* phospho-mutant embryos, the *Twist1*-expressing tissues are visibly reduced in size, including the maxillary process (Fig. 7B-E, white arrows), the medial and lateral nasal processes (Fig. 7B-E) and the visibly smaller first and second PAs (Fig. 7B-E, asterisks). The frontal view of E11.5 control embryos shows the correct juxtaposition of the medial and lateral nasal processes, whereas the *Hand1* phospho-mutant embryos show an obvious reduction of *Twist1*-expressing mesenchyme (black arrows) within both the lateral and medial nasal processes of *Hand1* phospho-mutant embryos (Fig. 7F-J) and in the sinus cavity (Fig. 7P-T, asterisks), suggesting a loss of tissue. As expression levels of *Twist1* mRNA do not appear uniformly reduced, we employed qRT-PCR analysis to quantitate the *Twist1* levels more accurately (Fig. 7U). Results show that indeed the levels of *Twist1* are significantly increased in both E10.5 *Hand1*$^{+/PO4-}$ and *Hand1*$^{+/PO4+}$. Thus, it appears that a loss of tissue is responsible for the altered *Twist1* expression pattern and that *Twist1* expression in both the remaining NCC- and non-NCC-derived mesenchyme is increased in *Hand1* phospho-mutants.

Development (2014) 141, 3050-3061 doi:10.1242/dev.107680

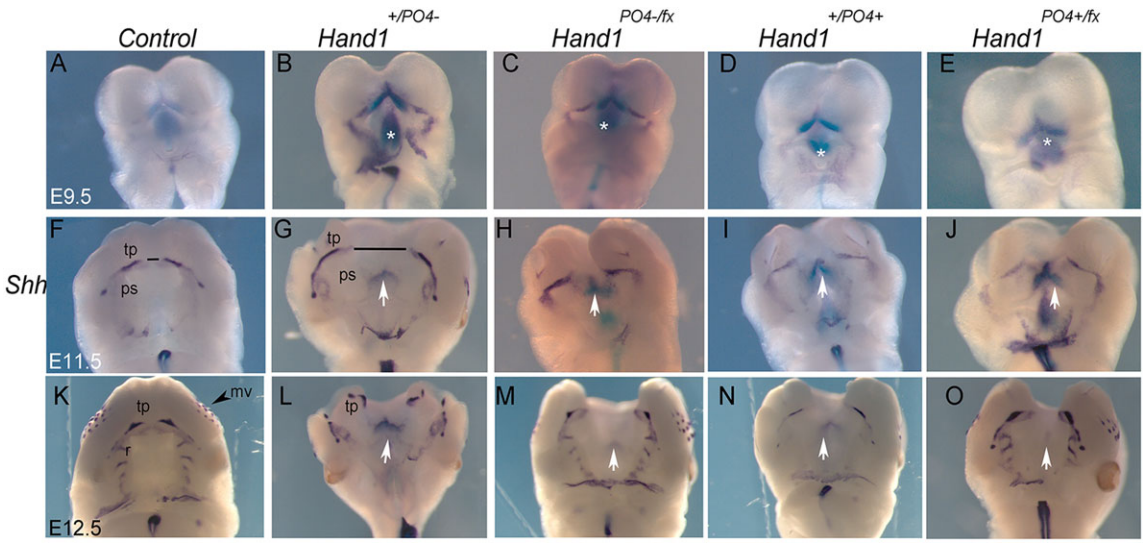

Fig. 5. *Shh* craniofacial expression in *Hand1* phospho-mutant embryos in ventral view. At E9.5 (A-E), E11.5 (F-J) and E12.5 (K-O), control (A,F,K), *Hand1*$^{+/PO4-}$ (B,G,L), *Hand1*$^{PO4-/fx}$ (C,H,M), *Hand1*$^{+/PO4+}$ (D,I,N) and *Hand1*$^{PO4+/fx}$ (E,J,O) were assayed for *Shh* expression by whole-mount ISH. White asterisks indicate enhanced *Shh* expression in the medial head mesenchyme at E9.5 (B-E). (F-O) By E11.5, *Shh* expression is restricted to the tooth primordia (tp) and esophagus (es) of control embryos. White arrows indicate persistent *Shh* expression in mutant embryos both at E11.5 and E12.5. *Shh* expression in control mystacial vibrissae (mv, black arrowhead) and rugae (r) is also observed normally in both controls and mutants (not visible). $n \geq 4$ for each genotype.

Inhibition of Shh signaling partially rescues *Hand1* phospho-mutant mid-face clefting

Given the upregulation of *Fgf8*, *Shh* and *Twist1*, we reasoned that we could improve the mid-face clefting phenotype by reducing the gene dosage of *Twist1*. To test this, we crossed the *Hand1*$^{+/PO4+}$; *Wnt1-Cre(+)* alleles onto the *Twist1*^{fx} allele and looked for improvement of mid-face clefting at E11.5 (Fig. 8A-F). Results show no improvement to mid-face clefting in *Hand1*$^{+/PO4+}$; *Twist1*$^{fx/+}$;*Wnt1-Cre(+)* embryos, and *Hand1*$^{+/PO4+}$;*Twist1*$^{fx/-}$; *Wnt1-Cre(+)* superimposes *Twist1*-mediated exencephaly (Chen and Behringer, 1995; Soo et al., 2002) on the *Hand1* phospho-mutant clefting phenotype (Fig. 8E,F). We also reasoned that *Hand2* expression levels could influence the *Hand1* phospho-mutant phenotypes. We therefore crossed *Hand1*$^{fx/PO4-}$;*Wnt1-Cre(+)* mice onto the *Hand2*$^{+/neo}$ background; however, lowering *Hand2* gene dosage had no visible effects on *Hand1* phospho-mutant craniofacial phenotypes (Fig. 8G-I).

We next reasoned that inhibition of Shh signaling could potentially improve *Hand1* phospho-mutant mid-face clefting, so we injected pregnant dams with cyclopamine (Kasberg et al., 2013; Lipinski et al., 2008) to antagonize Shh pathway activation and harvested embryos at E13.5 and E14.5 (Fig. 8J-U). Partial phenotype rescue is observed in the most severe *Hand1*$^{+/PO4-}$;*Wnt1-Cre(+)* mutant phenotype (three out of 15 mutant embryos isolated), as compared with the 100% penetrance of pronounced mid-face clefting observed in *Hand1*$^{+/PO4-}$;*Wnt1-Cre(+)* mice (Fig. 8I,L,M,R,S). The least severe *Hand1*$^{PO4+/fx}$;*Wnt1-Cre(+)* mutants show more efficient rescue (seven out of nine mutants; Fig. 8N,O,T,U). It is established that abnormally low and high levels of Shh can also result in facial abnormalities (Lipinski et al., 2010), and the improved phenotype observed further supports the notion that the increased Shh level observed in *Hand1* phospho-mutants contributes directly to the mid-face cleft phenotype.

DISCUSSION

The bHLH transcription factor Hand1 is clearly dispensable for craniofacial formation (Barbosa et al., 2007). However, altering the phosphoregulation of Hand1, which influences its bHLH dimerization, within the distal-most pharyngeal arch mesoderm results in a severe non-cell-autonomous increase in PA NCC death that ultimately manifests in a mid-face cleft phenotype. In addition to increased cell death, essential signaling pathways required for proper craniofacial morphogenesis (Fgf8 and Shh) show expanded expression in *Hand1* phospho-mutant embryos. Treatment *in utero* with the Shh antagonist cyclopamine can improve the severity of the resultant mid-face cleft (Fig. 8), thus supporting the hypothesis that the increases observed in these signaling pathways drive the resultant phenotype.

Hand1 expression is observed only within the most distal arch mesenchyme and becomes detectable between E9.0 and E9.5 (Fig. 1; Firulli et al., 1998; Ruest et al., 2004). As the *Hand1*$^{PO4-}$ and *Hand1*$^{PO4+}$ mutants are knock-in alleles, these Hand1 dimer mutants are expressed at endogenous levels in a spatio-temporal pattern consistent with wild-type *Hand1*. At E9.5, *Hand1* phospho-mutants display robust pathological cell death in the PAs, indicating that the deleterious effects from the expression of the mutant allele are nearly immediate within the arch mesenchyme. Indeed, phenotypic changes are present by E10.5 (supplementary material Fig. S1). Histological analysis indicates that right and left structures are essentially normal, although, due to the loss of tissue from the early cell death, the outgrowth of the right and left sides of the forming face fail to fuse (supplementary material Fig. S2). This conclusion is supported by the normal expression of the fusion markers jagged 2 (*Jag2*) and matrix metallopeptidase 13 (*Mmp13*) (supplementary material Fig. S4) and the direct initiation of fusion observed in *Hand1*$^{PO4+/fx}$;*Wnt1-Cre(+)* embryos (Fig. 1N; supplementary material Fig. S2), which exhibit the least amount of early cell death and a less severe phenotype. Additionally, by utilizing the *P0-Cre* mouse strain to activate *Hand1* mutant allele expression within the NCC during their migration [a full day later than *Wnt1-Cre* allelic activation (Yamauchi et al., 1999)], the severity and penetrance of the mid-face cleft is greatly reduced (supplementary material Fig. S6). This reinforces the idea that the deleterious effects of Hand1 phospho-mutant proteins are immediate to their expression and that even a subtle delay in expression largely limits

Development (2014) 141, 3050-3061 doi:10.1242/dev.107680

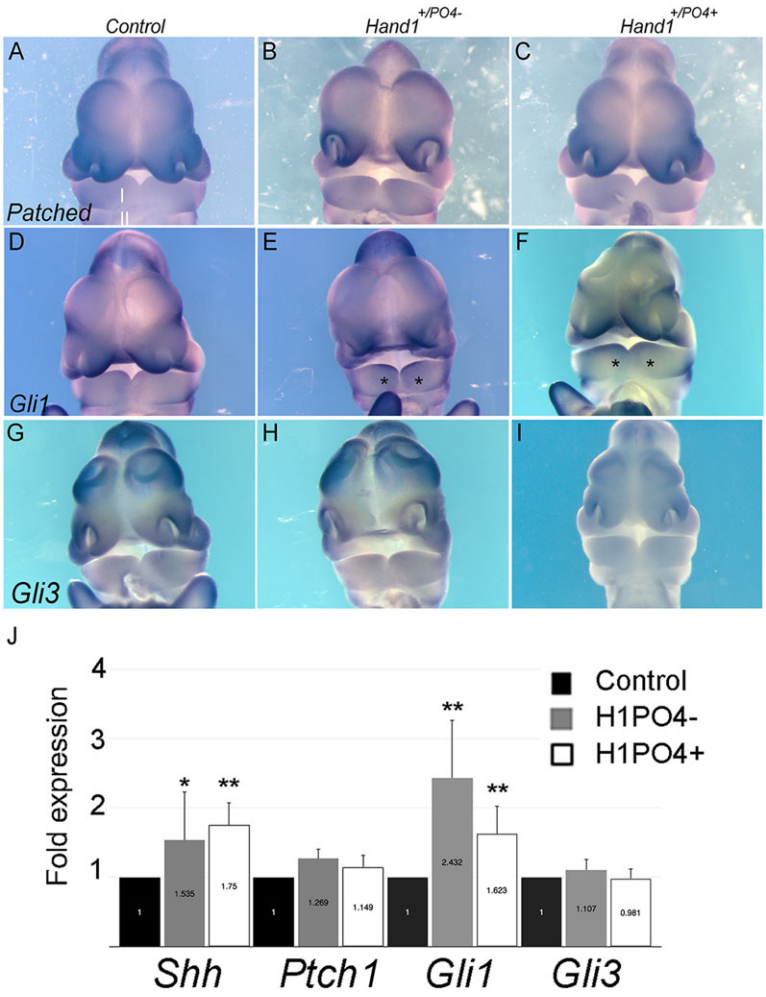

Fig. 6. Expression of *Shh* downstream responders *Ptch1*, *Gli1* and *Gli3* expression in E10.5 control and *Hand1* phospho-mutant embryos. (A-C) *Ptch1* expression appears unaffected in the first pharyngeal arch. (D-F) *Gli1* expression within the first pharyngeal arch is also enhanced (marked by asterisks). (G-I) Comparison of *Gli3* expression between control and *Hand1* phospho-mutant embryos reveals no significant changes in expression. (J) qRT-PCR analysis of *Shh*, *Ptch1*, *Gli1* and *Gli3* expression. Error bars denote s.e.m.; $*P \leq 0.05$ and $**P \leq 0.01$ by Student's *t*-test. $n \geq 4$ for each genotype.

the observed phenotype. Combined, these data demonstrate that *Hand1* phospho-mutant facial structures are capable of fusion and, considering the lack of significant changes in cell proliferation, suggest that a non-cell-autonomous increase in arch mesenchyme cell death causes these phenotypes. Given that reduced cell death is observed in the distal most arch mesenchyme where the *Hand1* dimer mutants are expressed (Fig. 2), it is probable that Hand1 phospho-mutants interfere with other bHLH dimer choices within this limited *Hand1* expression domain. Consequently, this causes the non-cell-autonomous cell death, leading directly to the changes in Fgf8 and Shh signaling pathway expression and ultimately resulting in the defects in the upper bones of the skull. Outside the *Hand1* expression domain, we observe a loss of *Twist1*-expressing tissue but an increase in *Twist1* expression (Fig. 7), which could lead to increased formation of Twist1 homodimers. Indeed, increased Twist1 homodimer expression is directly associated with premature ossification and suture fusion accompanied by enhanced Fgf signaling (Connerney et al., 2006, 2008). Conversely, later-stage deletion of *Twist1* using *Tyr-Cre* also yields a mid-faced cleft (Bildsoe et al., 2009), reinforcing the notion that altered gene dosage in conjunction with dimer choice can dramatically effect development. In genetic experiments, lowering the gene dosage of *Twist1* on the $Hand1^{+/PO4-}$ background does not improve the mid-face phenotype, and complete NCC conditional knockout of Twist1 on the $Hand1^{+/PO4-}$ via *Wnt1-Cre* results in a more severe phenotype than either mutant separately (Fig. 8).

Another possible interpretation of these findings is that a bHLH-dependent distal arch-signaling center could integrate Fgf8 and Shh signaling pathways. The incongruity of the tightly restricted domain of *Hand1* within the distal midline of the first mandibular PA and the alterations in gene expression observed in *Hand1* phosphoregulation mutants is consistent with the 'Hinge and Caps' model proposed by Depew (Compagnucci et al., 2013; Depew and Compagnucci, 2008; Depew and Simpson, 2006; Fish et al., 2011). In this model, reciprocal signaling between the putative 'Hinge', or the oral ectoderm of the proximal first PA, and two 'Caps' [corresponding to (1) the medial frontonasal processes and (2) the distal mandibular midline] pattern the nascent jaw along the proximo-distal, medio-lateral and rostro-caudal axes. This reciprocal signaling could explain how altered bHLH-dependent transcriptional mechanisms within the distal mandibular midline can alter gene expression profiles non-cell autonomously within the medial frontonasal processes and cause ectopic cell death within the proximal first arch. We can rule out the alternative possibility of cell migration from regions of *Hand1* expression in the mandibular arch to the maxillary prominence, as $Hand1^{Cre}$ lineage analysis shows that *Hand1* daughter cells do not enter the maxillary prominence (Barnes et al., 2010).

Initially, we were surprised by the observation that both the hypophosphorylated and phosphorylation-mimicking *Hand1* mutants exhibit a less severe phenotype when the wild-type *Hand1* allele is deleted. This observation highlights the mechanics of bHLH factors and their prerequisite homodimer or heterodimer formation conveying transcriptional activity on target genes. It is clear that complete

Development (2014) 141, 3050-3061 doi:10.1242/dev.107680

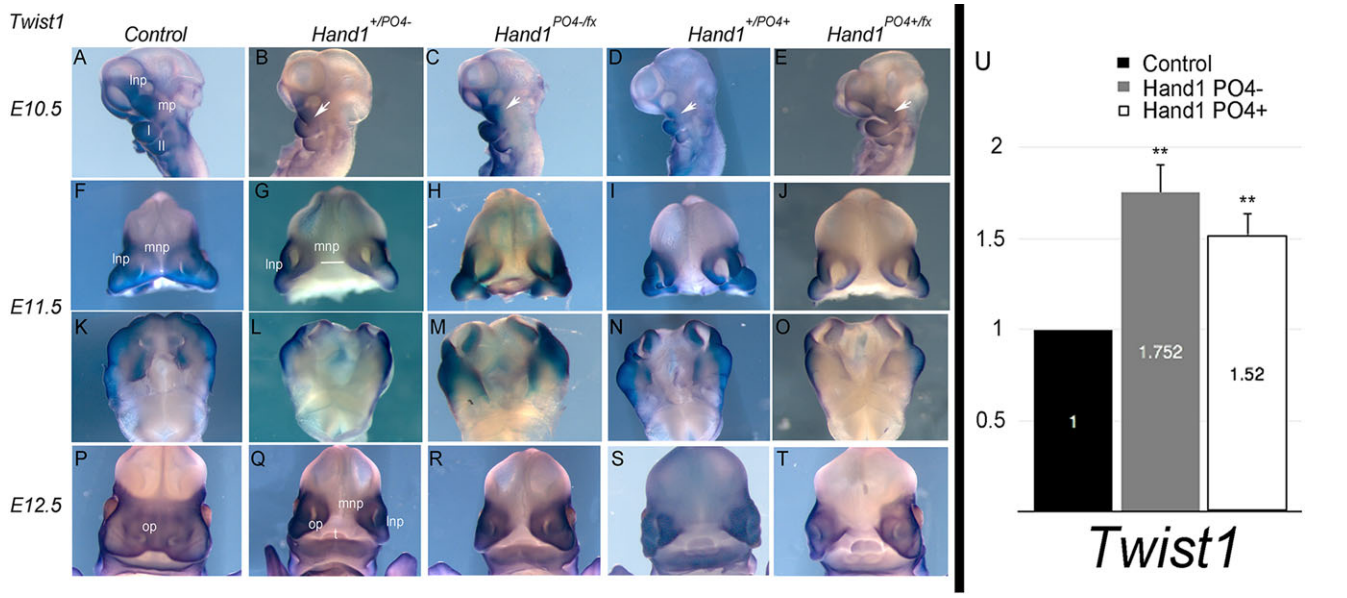

Fig. 7. *Twist1* craniofacial expression in *Hand1* phospho-mutant embryos. At E10.5 (A-E), E11.5 (F-O) and E12.5 (P-T), control (A,F,K,P), $Hand1^{+/PO4-}$ (B,G,L,Q), $Hand1^{PO4-/fx}$ (C,H,M,R), $Hand1^{+/PO4+}$ (D,J,N,S) and $Hand1^{PO4+/fx}$ (E,J,O,T) were assayed for *Twist1* expression by whole-mount ISH. (A) E10.5 control, embryos show strong *Twist1* expression within the lateral nasal process (lnp) and maxillary process (mp), as well as first (I) and second (II) PAs. (B-E) In *Hand1* phospho-mutants, *Twist1* expression is visibly reduced within both PAs and the maxillary process (white arrow). Frontal views of E11.5 control (F) and mutant (G-J) embryos show a reduced level of expression within the medial nasal process (mnp) as well as a loss of medial expression between the olfactory pits (demonstrated by white line in G). Ventral views of F-J show *Twist1* expression within the head mesenchyme. E12.5 control (P) and *Hand1* phospho-mutant heads (Q-T). (U) qRT-PCR analysis of *Twist1* expression. Error bars denote s.e.m.; $*P \leq 0.05$ and $**P \leq 0.01$ by Student's *t*-test. $n \geq 4$ for each genotype.

deletion of *Hand1* does not significantly affect the bHLH dimer pool within the distal mesenchyme, as such *Hand1* loss-of-function mutants are phenotypically normal, viable and fertile (Barbosa et al., 2007). The absence of *Hand1*-mediated defects might be the result of functional compensation by the related bHLH factor Hand2 within the cranial NCC. This is an established mechanism that functions in both sympathetic neurons and the developing heart (Barbosa et al., 2007; Hendershot et al., 2008; Howard, 2005; McFadden et al., 2005; Vincentz et al., 2012). By contrast, altering Hand1 phosphoregulation alters the ability of Hand1 to interact with potential bHLH dimer partners (Firulli et al., 2003). By interfering with the function of other crucial bHLH factors via direct dimerization and/or by titration of available E-protein levels, the result is a dramatic increase in PA cell death. The finding that wild-type Hand1, in the presence of the *Hand1* phospho-mutant alleles, contributes to these deleterious transcriptional effects when the bHLH dimer pool is altered further confirms the role of *Hand* gene dosage phenotypes that are well established in a number of developmental systems, including the heart and limbs (Barbosa et al., 2007; Firulli et al., 2010, 2005; McFadden et al., 2005). The complexity of regulating the bHLH pool lies in determining all combinations of Hand bHLH dimer complexes within the extremely narrow temporal window when this dysfunction is occurring. Additionally, we have to consider that altering the Twist-family dimer regulation also affects DNA-binding affinities (Firulli et al., 2007). Therefore, it is also possible that Hand1 mutant proteins could target promoters inappropriately and/or facilitate other bHLH factors to do likewise, thus further effecting gene expression.

MATERIALS AND METHODS

Mouse strains, genotyping and cyclopamine injections

$Hand1^{stopfloxHand1T107;S109A}$ ($Hand1^{PO4-}$) and $Hand1^{stopfloxHand1T107;S109D}$ ($Hand1^{PO4+}$) mice were generated from embryonic stem cells targeted with the constructs described in Fig. 1. Genotyping was performed by Southern blot as described previously (Firulli et al., 1998), or with the allele-specific primers H1 (5′-CTGCCATTGGCTCCGGCTAGAGGT-3′) and PGK (5′-GGCTGCTAAAGCGCATGCTCCAGACTG-3′), using PCR conditions of 94°C for 1 min, 60°C for 1 min and 72°C for 1 min for 35 cycles. B6.129S4-*Gt (ROSA)26Sortm1Sor*/J (*ROSA26R-β-gal* homozygous; $R26R^{lacZ}$) mice were genotyped using a probe located 5′ of the Stop-Flox (provided by Dr Phillippe Soriano, Mount Sinai Hospital). Both $Hand1^{+/PO4-}$ and $Hand1^{+/PO4+}$ alleles were bred onto a $R26R^{lacZ}$ homozygous background, and females of this genotype were crossed to *Wnt1-Cre* [*Tg(Wnt1-cre)2Sor*] (Danielian et al., 1998) or *Wnt1-Cre(+)*;$Hand1^{fx/fx}$ males to generate either $Hand1^{+/PO4}$ or $Hand1^{fx/PO4}$ embryos. *RARE-lacZ* mice [*Tg(RARE-Hspa1b/lacZ)*12Jrt/J] were obtained from the Jackson Laboratories. *P0-Cre* mice (Yamauchi et al., 1999) were obtained from Simon J. Conway (Indiana University, USA). Cyclopamine (Sigma) was resuspended at 1 mg/ml in 45% w/v solution in water 2-hydroxpropyl-beta-cyclodextrin solution and administered at a dosage of 20 mg/kg bodyweight twice daily to pregnant dams at E8.5-E10.5 via intraperitoneal injection.

Histology

Embryos (E9.5-E18.5) were fixed in 4% paraformaldehyde, dehydrated, embedded, sectioned and Hematoxylin and Eosin (H&E) stained as described (Firulli et al., 2010). A minimum of four viable embryos per genotype was used for all analyses. All data were collected on a Leica DM5000 B compound fluorescence microscope.

ISH-qRT-PCR

Digoxygenin (DiG)-labeled section and whole-mount ISHs were carried out as described (Barnes et al., 2011; Firulli et al., 2010; Vincentz et al., 2008). qRT-PCR was performed on a LightCycler 480II (Roche) using TaqMan primers (Life Technologies) recognizing the following transcripts: *Fgf8*, *Spry1*, *Fgfr1*, *Etv5*, *Etv4*, *Shh*, *Ptch1*, *Gli1*, *Gli3* and *Twist1*. Heads cut between the first and second PAs from viable embryos were flash-frozen for RNA isolation and genotyped from the yolk sac DNA. Total RNA was isolated using a High Pure RNA Tissue Kit (Roche) and cDNA was prepared using a High-Capacity cDNA Reverse Transcription Kit (Life Technologies) following the manufacturer's protocol. Error bars denote s.e.m. Statistical significance was determined using Student's *t*-test. *P*-values ≤ 0.05 were regarded as significant and marked in all graphs by a

Development (2014) 141, 3050-3061 doi:10.1242/dev.107680

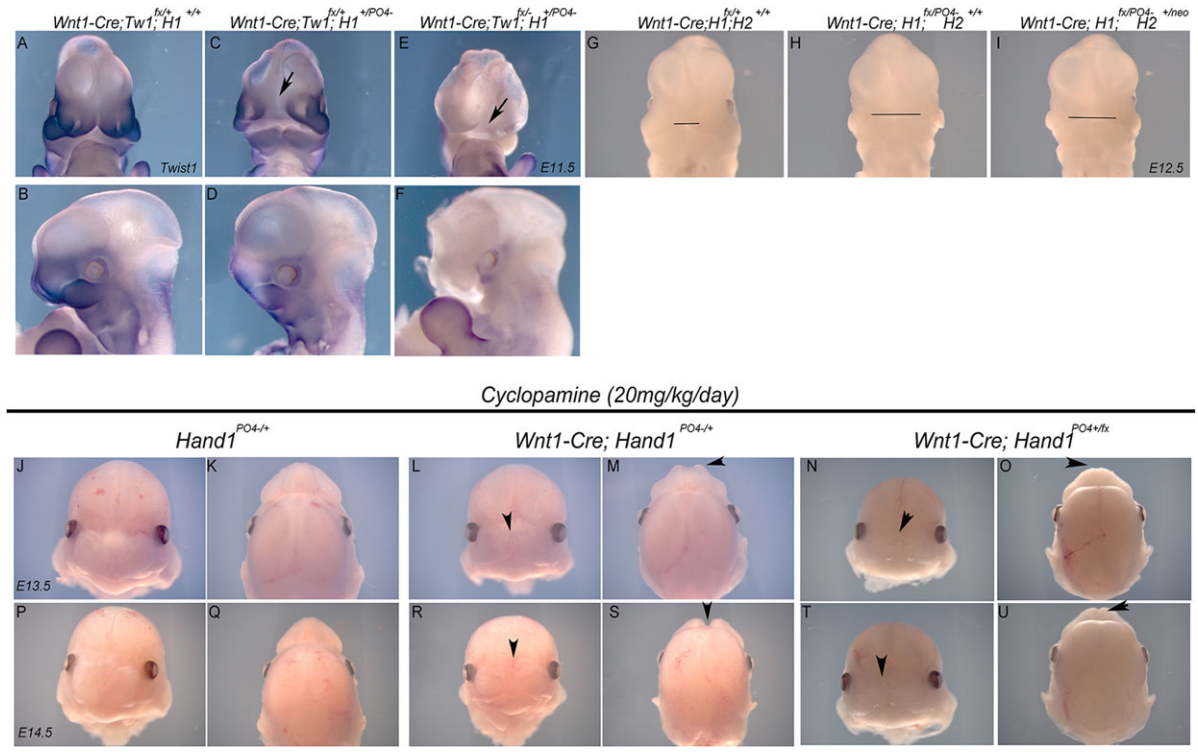

Fig. 8. *Twist1* loss-of-function does not impact on *Hand1* phospho-mutant-mediated mid-face clefting, but antagonism of Shh activity improves phenotype. (A-F) *Twist1* ISH on control (A,B), *Hand1*$^{+/PO4-}$;*Twist1*$^{fx/+}$;*Wnt1-Cre*(+) (C,D) and *Hand1*$^{+/PO4-}$;*Twist1*$^{fx/-}$;*Wnt1-Cre*(+) (E,F). Lower gene dosage of *Twist1* does not improve *Hand1* phospho-mutant mid-face clefting (black arrows). (G-I) *Hand2* loss-of-function does not impact on *Hand1* phospho-mutant-mediated mid-face clefting. Bars indicate distance between nasal pits. (J-U) *In utero* cyclopamine (20 mg/kg/day) treatment improves mid-face clefting. Fifteen *Wnt1-Cre*;*Hand1*$^{+/PO4-}$ mutant embryos and nine *Wnt1-Cre*;*Hand1*$^{PO4+/fx}$ were isolated at E13.5 (J-O) or E14.5 (P-U) after daily treatments with cyclopamine between E9.5 and E10.5. Improved craniofacial formation is observed in three of the 15 *Hand1*$^{+/PO4}$ mutants (L,M,R,S, black arrowheads) and in seven out of nine *Hand1*$^{PO4+/fx}$ mutants (N,O,T,U, black arrowheads). Control mice (G,H,M,N) also display mild morphological defects from the alteration of Shh activity.

single asterisk, and *P*-values ≤0.01 are denoted by a double asterisk. $n \geq 4$ in all experiments.

TUNEL, LysoTracker and EdU immunohistochemistry analysis

TUNEL analysis on sectioned embryos was performed as described (Firulli et al., 2010). LysoTracker (Life Technologies) was incubated with embryos as per the manufacturer's instructions. Embryos were imaged in a well slide. Cell proliferation was assayed using the Click-IT EdU Imaging Kit (Life Technologies). Pregnant dams were injected with EdU (200 mg/kg body weight) 1 h prior to embryo harvest.

Micro-CT and skeletal preparations

Craniofacial morphology of P0 mice was assessed using high-resolution desktop X-ray microtomography (micro-CT) SkyScan 1172 imaging system (SkyScan). Skulls were dissected, fixed in 10% neutral buffered formalin and stored in 70% ethanol. Skulls were scanned with an isotropic voxel size of 8 µm, with an energy level of 50 kV and an aluminum 0.5 mm filter. A lower energy source was used to capture regions of undermineralized bone. Two-dimensional (2D) cross-sectional grayscale slices (~600-800 slices per skull) from each skull were reconstructed using NRecon reconstruction software (SkyScan). Reconstructed slices were saved as individual TIFF images and converted to a DICOM (Digital Imaging and Communications in Medicine) format. DICOM files were used to create 3D models using OsiriX version 5.6, imaging processing software for DICOM images (Medical Imaging Software). All 3D images were created using identical grayscale thresholds, with scaling of each image conserved. Overlaying skeletal structures were removed using a bone removal tool to identify structures of the palate (Fig. 1). $n \geq 4$ per genotype scanned and reconstructed. Measurements of bones were performed on all scanned heads and significance ($P \leq 0.05$) determined by Student's *t*-test. Skeletal preparations were performed as described (Firulli et al., 2005).

Acknowledgements

We thank Danny Carney for technical assistance. Infrastructural support at the Herman B Wells Center for Pediatric Research is in part supported by the generosity of the Riley Children's Foundation, and the Carrolton Buehl McCulloch Chair of Pediatrics.

Competing interests

The authors declare no competing financial interests.

Author contributions

B.A.F. designed and performed experiments, wrote and edited the manuscript. R.K.F. performed micro-CT analysis. J.W.V. performed data interpretation and consultation in experiment design. D.E.C. performed data interpretation and consultation, wrote and edited the manuscript. A.B.F. designed and performed experiments, performed data interpretation, wrote and edited the manuscript.

Funding

This work was supported by the National Institutes of Health (NIH) [1R0AR061392-03]. Deposited in PMC for release after 12 months.

Supplementary material

Supplementary material available online at
http://dev.biologists.org/lookup/suppl/doi:10.1242/dev.107680/-/DC1

References

Abe, M., Maeda, T. and Wakisaka, S. (2008). Retinoic acid affects craniofacial patterning by changing Fgf8 expression in the pharyngeal ectoderm. *Dev. Growth Differ.* **50**, 717-729.

Abzhanov, A. and Tabin, C. J. (2004). Shh and Fgf8 act synergistically to drive cartilage outgrowth during cranial development. *Dev. Biol.* **273**, 134-148.

Abzhanov, A., Cordero, D. R., Sen, J., Tabin, C. J. and Helms, J. A. (2007). Cross-regulatory interactions between Fgf8 and Shh in the avian frontonasal prominence. *Congenit. Anom. Kyoto* **47**, 136-148.

Barbosa, A. C., Funato, N., Chapman, S., McKee, M. D., Richardson, J. A., Olson, E. N. and Yanagisawa, H. (2007). Hand transcription factors

cooperatively regulate development of the distal midline mesenchyme. *Dev. Biol.* **310**, 154-168.
Barnes, R. M. and Firulli, A. B. (2009). A Twist of insight - the role of Twist-Family bHLH factors in development. *Int. J. Dev. Biol.* **53**, 909-924.
Barnes, R. M., Firulli, B. A., Conway, S. J., Vincentz, J. W. and Firulli, A. B. (2010). Analysis of the Hand1 cell lineage reveals novel contributions to cardiovascular, neural crest, extra-embryonic, and lateral mesoderm derivatives. *Dev. Dyn.* **239**, 3086-3097.
Barnes, R. M., Firulli, B. A., VanDusen, N. J., Morikawa, Y., Conway, S. J., Cserjesi, P., Vincentz, J. W. and Firulli, A. B. (2011). Hand2 loss-of-function in Hand1-expressing cells reveals distinct roles in epicardial and coronary vessel development. *Circ. Res.* **108**, 940-949.
Barron, F., Woods, C., Kuhn, K., Bishop, J., Howard, M. J. and Clouthier, D. E. (2011). Downregulation of Dlx5 and Dlx6 expression by Hand2 is essential for initiation of tongue morphogenesis. *Development* **138**, 2249-2259.
Bildsoe, H., Loebel, D. A. F., Jones, V. J., Chen, Y.-T., Behringer, R. R. and Tam, P. P. L. (2009). Requirement for Twist1 in frontonasal and skull vault development in the mouse embryo. *Dev. Biol.* **331**, 176-188.
Brugmann, S. A., Tapadia, M. D. and Helms, J. A. (2006). The molecular origins of species-specific facial pattern. *Curr. Top. Dev. Biol.* **73**, 1-42.
Cai, J. and Jabs, E. W. (2005). A twisted hand: bHLH protein phosphorylation and dimerization regulate limb development. *BioEssays* **27**, 1102-1106.
Castanon, I., Von Stetina, S., Kass, J. and Baylies, M. K. (2001). Dimerization partners determine the activity of the Twist bHLH protein during Drosophila mesoderm development. *Development* **128**, 3145-3159.
Chai, Y. and Maxson, R. E., Jr. (2006). Recent advances in craniofacial morphogenesis. *Dev. Dyn.* **235**, 2353-2375.
Chen, Z. F. and Behringer, R. R. (1995). Twist is required in head mesenchyme for cranial neural tube morphogenesis. *Genes Dev.* **9**, 686-699.
Chen, Y., Moon, A. M. and Gaufo, G. O. (2012). Influence of mesodermal Fgf8 on the differentiation of neural crest-derived postganglionic neurons. *Dev. Biol.* **361**, 125-136.
Clouthier, D. E., Williams, S. C., Yanagisawa, H., Wieduwilt, M., Richardson, J. A. and Yanagisawa, M. (2000). Signaling pathways crucial for craniofacial development revealed by endothelin-A receptor-deficient mice. *Dev. Biol.* **217**, 10-24.
Clouthier, D. E., Williams, S. C., Hammer, R. E., Richardson, J. A. and Yanagisawa, M. (2003). Cell-autonomous and nonautonomous actions of endothelin-A receptor signaling in craniofacial and cardiovascular development. *Dev. Biol.* **261**, 506-519.
Clouthier, D. E., Garcia, E. and Schilling, T. F. (2010). Regulation of facial morphogenesis by endothelin signaling: insights from mice and fish. *Am. J. Med. Genet. A* **152A**, 2962-2973.
Clouthier, D. E., Passos-Bueno, M. R., Tavares, A. L. P., Lyonnet, S., Amiel, J. and Gordon, C. T. (2013). Understanding the basis of auriculocondylar syndrome: insights from human, mouse and zebrafish genetic studies. *Am. J. Med. Genet. C Semin. Med. Genet.* **163**, 306-317.
Cobourne, M. T., Xavier, G. M., Depew, M., Hagan, L., Sealby, J., Webster, Z. and Sharpe, P. T. (2009). Sonic hedgehog signalling inhibits palatogenesis and arrests tooth development in a mouse model of the nevoid basal cell carcinoma syndrome. *Dev. Biol.* **331**, 38-49.
Compagnucci, C., Debiais-Thibaud, M., Coolen, M., Fish, J., Griffin, J. N., Bertocchini, F., Minoux, M., Rijli, F. M., Borday-Birraux, V., Casane, D. et al. (2013). Pattern and polarity in the development and evolution of the gnathostome jaw: both conservation and heterotopy in the branchial arches of the shark, Scyliorhinus canicula. *Dev. Biol.* **377**, 428-448.
Connerney, J., Andreeva, V., Leshem, Y., Muentener, C., Mercado, M. A. and Spicer, D. B. (2006). Twist1 dimer selection regulates cranial suture patterning and fusion. *Dev. Dyn.* **235**, 1334-1346.
Connerney, J., Andreeva, V., Leshem, Y., Mercado, M. A., Dowell, K., Yang, X., Lindner, V., Friesel, R. E. and Spicer, D. B. (2008). Twist1 homodimers enhance FGF responsiveness of the cranial sutures and promote suture closure. *Dev. Biol.* **318**, 323-334.
Danielian, P. S., Muccino, D., Rowitch, D. H., Michael, S. K. and McMahon, A. P. (1998). Modification of gene activity in mouse embryos in utero by a tamoxifen-inducible form of Cre recombinase. *Curr. Biol.* **8**, 1323-1326.
Depew, M. J. and Compagnucci, C. (2008). Tweaking the hinge and caps: testing a model of the organization of jaws. *J. Exp. Zoolog. B Mol. Dev. Evol.* **310B**, 315-335.
Depew, M. J. and Simpson, C. A. (2006). 21st century neontology and the comparative development of the vertebrate skull. *Dev. Dyn.* **235**, 1256-1291.
Firnberg, N. and Neubüser, A. (2002). FGF signaling regulates expression of Tbx2, Erm, Pea3, and Pax3 in the early nasal region. *Dev. Biol.* **247**, 237-250.
Firulli, A. B. and Conway, S. J. (2008). Phosphoregulation of Twist1 provides a mechanism of cell fate control. *Curr. Med. Chem.* **15**, 2641-2647.
Firulli, A. B., McFadden, D. G., Lin, Q., Srivastava, D. and Olson, E. N. (1998). Heart and extra-embryonic mesodermal defects in mouse embryos lacking the bHLH transcription factor Hand1. *Nat. Genet.* **18**, 266-270.
Firulli, B., Howard, M. J., McDaid, J. R., McIlreavey, L., Dionne, K. M., Centonze, V., Cserjesi, P., Virshup, D. M. and Firulli, A. B. (2003). PKA, PKC and the protein phosphatase 2A influence HAND factor function: a mechanisms for tissue specific transcriptional regulation. *Mol. Cell* **12**, 1225-1237.
Firulli, B. A., Krawchuk, D., Centonze, V. E., Vargesson, N., Virshup, D. E., Conway, S. J., Cserjesi, P., Laufer, E. and Firulli, A. B. (2005). Altered Twist1 and Hand2 dimerization is associated with Saethre-Chotzen syndrome and limb abnormalities. *Nat. Genet.* **37**, 373-381.
Firulli, B. A., Redick, B. A., Conway, S. J. and Firulli, A. B. (2007). Mutations within helix I of Twist1 result in distinct limb defects and variation of DNA binding affinities. *J. Biol. Chem.* **282**, 27536-27546.
Firulli, B. A., McConville, D. P., Byers, J. S., III, Vincentz, J. W., Barnes, R. M. and Firulli, A. B. (2010). Analysis of a Hand1 hypomorphic allele reveals a critical threshold for embryonic viability. *Dev. Dyn.* **239**, 2748-2760.
Fish, J. L., Villmoare, B., Köbernick, K., Compagnucci, C., Britanova, O., Tarabykin, V. and Depew, M. J. (2011). Satb2, modularity, and the evolvability of the vertebrate jaw. *Evol. Dev.* **13**, 549-564.
Gitton, Y., Heude, E., Vieux-Rochas, M., Benouaiche, L., Fontaine, A., Sato, T., Kurihara, Y., Kurihara, H., Couly, G. and Levi, G. (2010). Evolving maps in craniofacial development. *Semin. Cell Dev. Biol.* **21**, 301-308.
Griffin, J. N., Compagnucci, C., Hu, D., Fish, J., Klein, O., Marcucio, R. and Depew, M. J. (2013). Fgf8 dosage determines midfacial integration and polarity within the nasal and optic capsules. *Dev. Biol.* **374**, 185-197.
Hendershot, T. J., Liu, H., Clouthier, D. E., Shepherd, I. T., Coppola, E., Studer, M., Firulli, A. B., Pittman, D. L. and Howard, M. J. (2008). Conditional deletion of Hand2 reveals critical functions in neurogenesis and cell type-specific gene expression for development of neural crest-derived noradrenergic sympathetic ganglion neurons. *Dev. Biol.* **319**, 179-191.
Hornik, C., Brand-Saberi, B., Rudloff, S., Christ, B. and Füchtbauer, E.-M. (2004). Twist is an integrator of SHH, FGF, and BMP signaling. *Anat. Embryol.* **209**, 31-39.
Howard, M. J. (2005). Mechanisms and perspectives on differentiation of autonomic neurons. *Dev. Biol.* **277**, 271-286.
Hu, D., Marcucio, R. S. and Helms, J. A. (2003). A zone of frontonasal ectoderm regulates patterning and growth in the face. *Development* **130**, 1749-1758.
Huang, X., Litingtung, Y. and Chiang, C. (2007). Ectopic sonic hedgehog signaling impairs telencephalic dorsal midline development: implication for human holoprosencephaly. *Hum. Mol. Genet.* **16**, 1454-1468.
Jabs, E. W. (2004). TWIST and Saethre-Chotzen syndrome. In *Inborn Errors of Development* (ed. C. J. Epstein, R. P. Erickson and A. Wynshaw-Boris), pp. 401-409. New York: Oxford University Press.
Jeong, J., Mao, J., Tenzen, T., Kottmann, A. H. and McMahon, A. P. (2004). Hedgehog signaling in the neural crest cells regulates the patterning and growth of facial primordia. *Genes Dev.* **18**, 937-951.
Jiang, R., Bush, J. O. and Lidral, A. C. (2006). Development of the upper lip: morphogenetic and molecular mechanisms. *Dev. Dyn.* **235**, 1152-1166.
Kasberg, A. D., Brunskill, E. W. and Steven Potter, S. (2013). SP8 regulates signaling centers during craniofacial development. *Dev. Biol.* **381**, 312-323.
Kurihara, Y., Kurihara, H., Maemura, K., Kuwaki, T., Kumada, M. and Yazaki, Y. (1995). Impaired development of the thyroid and thymus in endothelin-1 knockout mice. *J. Cardiovasc. Pharmacol.* **26**, S13-S16.
Lan, Y. and Jiang, R. (2009). Sonic hedgehog signaling regulates reciprocal epithelial-mesenchymal interactions controlling palatal outgrowth. *Development* **136**, 1387-1396.
Lipinski, R. J., Hutson, P. R., Hannam, P. W., Nydza, R. J., Washington, I. M., Moore, R. W., Girdaukas, G. G., Peterson, R. E. and Bushman, W. (2008). Dose- and route-dependent teratogenicity, toxicity, and pharmacokinetic profiles of the hedgehog signaling antagonist cyclopamine in the mouse. *Toxicol. Sci.* **104**, 189-197.
Lipinski, R. J., Song, C., Sulik, K. K., Everson, J. L., Gipp, J. J., Yan, D., Bushman, W. and Rowland, I. J. (2010). Cleft lip and palate results from Hedgehog signaling antagonism in the mouse: phenotypic characterization and clinical implications. *Birth Defects Res. A Clin. Mol. Teratol.* **88**, 232-240.
Lunn, J. S., Fishwick, K. J., Halley, P. A. and Storey, K. G. (2007). A spatial and temporal map of FGF/Erk1/2 activity and response repertoires in the early chick embryo. *Dev. Biol.* **302**, 536-552.
Macatee, T. L., Hammond, B. P., Arenkiel, B. R., Francis, L., Frank, D. U. and Moon, A. M. (2003). Ablation of specific expression domains reveals discrete functions of ectoderm- and endoderm-derived FGF8 during cardiovascular and pharyngeal development. *Development* **130**, 6361-6374.
Massari, M. E. and Murre, C. (2000). Helix-loop-helix proteins: regulators of transcription in Eucaryotic organisms. *Mol. Cell. Biol.* **20**, 429-440.
McFadden, D. G., Barbosa, A. C., Richardson, J. A., Schneider, M. D., Srivastava, D. and Olson, E. N. (2005). The Hand1 and Hand2 transcription factors regulate expansion of the embryonic cardiac ventricles in a gene dosage-dependent manner. *Development* **132**, 189-201.
Minoux, M. and Rijli, F. M. (2010). Molecular mechanisms of cranial neural crest cell migration and patterning in craniofacial development. *Development* **137**, 2605-2621.
Minowada, G., Jarvis, L. A., Chi, C. L., Neubuser, A., Sun, X., Hacohen, N., Krasnow, M. A. and Martin, G. R. (1999). Vertebrate Sprouty genes are induced

Development (2014) 141, 3050-3061 doi:10.1242/dev.107680

by FGF signaling and can cause chondrodysplasia when overexpressed. *Development* **126**, 4465-4475.

Moon, A. M. and Capecchi, M. R. (2000). Fgf8 is required for outgrowth and patterning of the limbs. *Nat. Genet.* **26**, 455-459.

Noden, D. M. and Trainor, P. A. (2005). Relations and interactions between cranial mesoderm and neural crest populations. *J. Anat.* **207**, 575-601.

Raible, F. and Brand, M. (2001). Tight transcriptional control of the ETS domain factors Erm and Pea3 by Fgf signaling during early zebrafish development. *Mech. Dev.* **107**, 105-117.

Rossant, J., Zirngibl, R., Cado, D., Shago, M. and Giguere, V. (1991). Expression of a retinoic acid response element-hsplacZ transgene defines specific domains of transcriptional activity during mouse embryogenesis. *Genes Dev.* **5**, 1333-1344.

Ruest, L.-B. and Clouthier, D. E. (2009). Elucidating timing and function of endothelin-A receptor signaling during craniofacial development using neural crest cell-specific gene deletion and receptor antagonism. *Dev. Biol.* **328**, 94-108.

Ruest, L.-B., Xiang, X., Lim, K.-C., Levi, G. and Clouthier, D. E. (2004). Endothelin-A receptor-dependent and -independent signaling pathways in establishing mandibular identity. *Development* **131**, 4413-4423.

Sandell, L. L., Sanderson, B. W., Moiseyev, G., Johnson, T., Mushegian, A., Young, K., Rey, J.-P., Ma, J.-x., Staehling-Hampton, K. and Trainor, P. A. (2007). RDH10 is essential for synthesis of embryonic retinoic acid and is required for limb, craniofacial, and organ development. *Genes Dev.* **21**, 1113-1124.

Soo, K., O'Rourke, M. P., Khoo, P.-L., Steiner, K. A., Wong, N., Behringer, R. R. and Tam, P. P. L. (2002). Twist function is required for the morphogenesis of the cephalic neural tube and the differentiation of the cranial neural crest cells in the mouse embryo. *Dev. Biol.* **247**, 251-270.

Stoler, J. M., Rogers, G. F. and Mulliken, J. B. (2009). The frequency of palatal anomalies in Saethre-Chotzen syndrome. *Cleft Palate Craniofac. J.* **46**, 280-284.

Trainor, P. A. (2005). Specification and patterning of neural crest cells during craniofacial development. *Brain Behav. Evol.* **66**, 266-280.

Vincentz, J. W., Barnes, R. M., Rodgers, R., Firulli, B. A., Conway, S. J. and Firulli, A. B. (2008). An absence of Twist1 results in aberrant cardiac neural crest morphogenesis. *Dev. Biol.* **320**, 131-139.

Vincentz, J. W., VanDusen, N. J., Fleming, A. B., Rubart, M., Firulli, B. A., Howard, M. J. and Firulli, A. B. (2012). A Phox2- and Hand2-dependent Hand1 cis-regulatory element reveals a unique gene dosage requirement for Hand2 during sympathetic neurogenesis. *J. Neurosci.* **32**, 2110-2120.

Yamauchi, Y., Abe, K., Mantani, A., Hitoshi, Y., Suzuki, M., Osuzu, F., Kuratani, S. and Yamamura, K.-i. (1999). A novel transgenic technique that allows specific marking of the neural crest cell lineage in mice. *Dev. Biol.* **212**, 191-203.

Supplementary Figure 1: Wholemount views of *control* (A-F), *Hand1*$^{+/PO4-}$ (G-L), *Hand1*$^{PO4-/fx}$ (M-R), *Hand1*$^{+/PO4+}$ (S-X), and *Hand1*$^{PO4+/fx}$ (Y-Zd) embryos between E10.5 and E18.5. At E10.5 visible differences in facial structures are observed between *controls* (A) and phospho mutants (G, M, S, Y) including measure of the distance between the olfactory pits (op; black lines), size of maxillary process (mp) and frontal, lateral and distal nasal processes (fnp, lnp, mnp) though no significant difference is observed in mandible (md) size. In E11.5 controls (B) the left and right distal nasal process begins to meet at the midline, bringing the olfactory pits closer together. In *Hand1* phospho mutants (H, N, T, Z) the distance between the olfactory pits does not decrease. The extent of mid-face clefting is patently obvious at E12.5 (compare C with I, O, U, Za) where the tongue (t) is clearly visible through the cleft. Facial defects progressively become more pronounced at E14.5 (compare D with J, P, V, Zb). Top view of E18.5 *controls* (E) show the nasal capsule (nc) completely fused where as phospho mutants maintain unfused nasal capsules (K, Q, W, Zc asterisks). Ventral views reveal a near complete loss of the secondary palate (compare F with L, R, X, Zd; black arrows). n≥4 for each genotype.

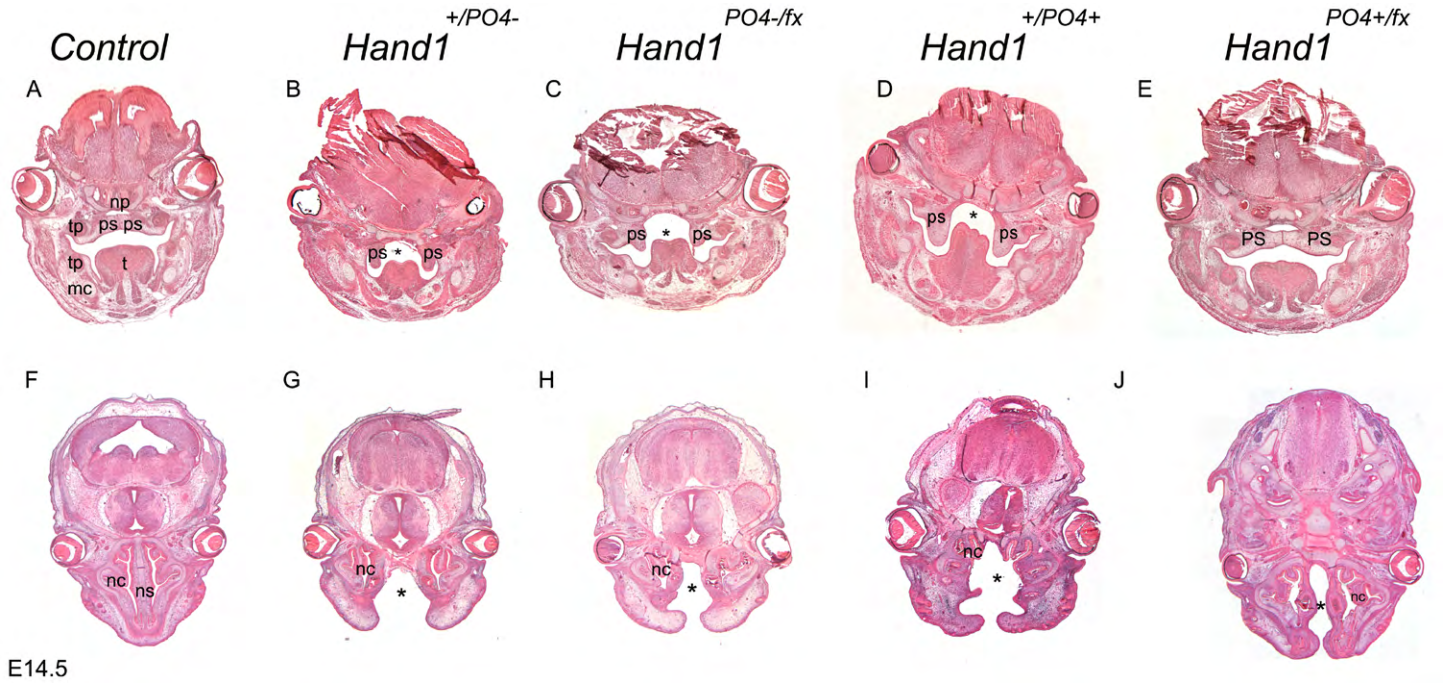

Supplementary Figure 2: Histological analysis of Hand1 phospho mutants at E14.5. Frontal (A-E) and transverse (F-J) sections of *Control* (A, F) *Hand1*$^{+/PO4-}$ (B, G), *Hand1*$^{PO4-/fx}$ (C, H), *Hand1*$^{+/PO4+}$ (D, I), and *Hand1*$^{PO4+/fx}$ (E, J) embryos. Frontal sections show that the tongue (t) fails to drop and that the palatal shelves (ps) fail to fuse (marked by asterisk). Tooth Primordia (tp) meckel's cartilage (mc) and other structures appear normally formed albeit displaced in location. Transverse sections show that the nasal cavities (nc) form in the phospho mutants; however, the nasal septum is absent from facial structures. n≥4 for each genotype.

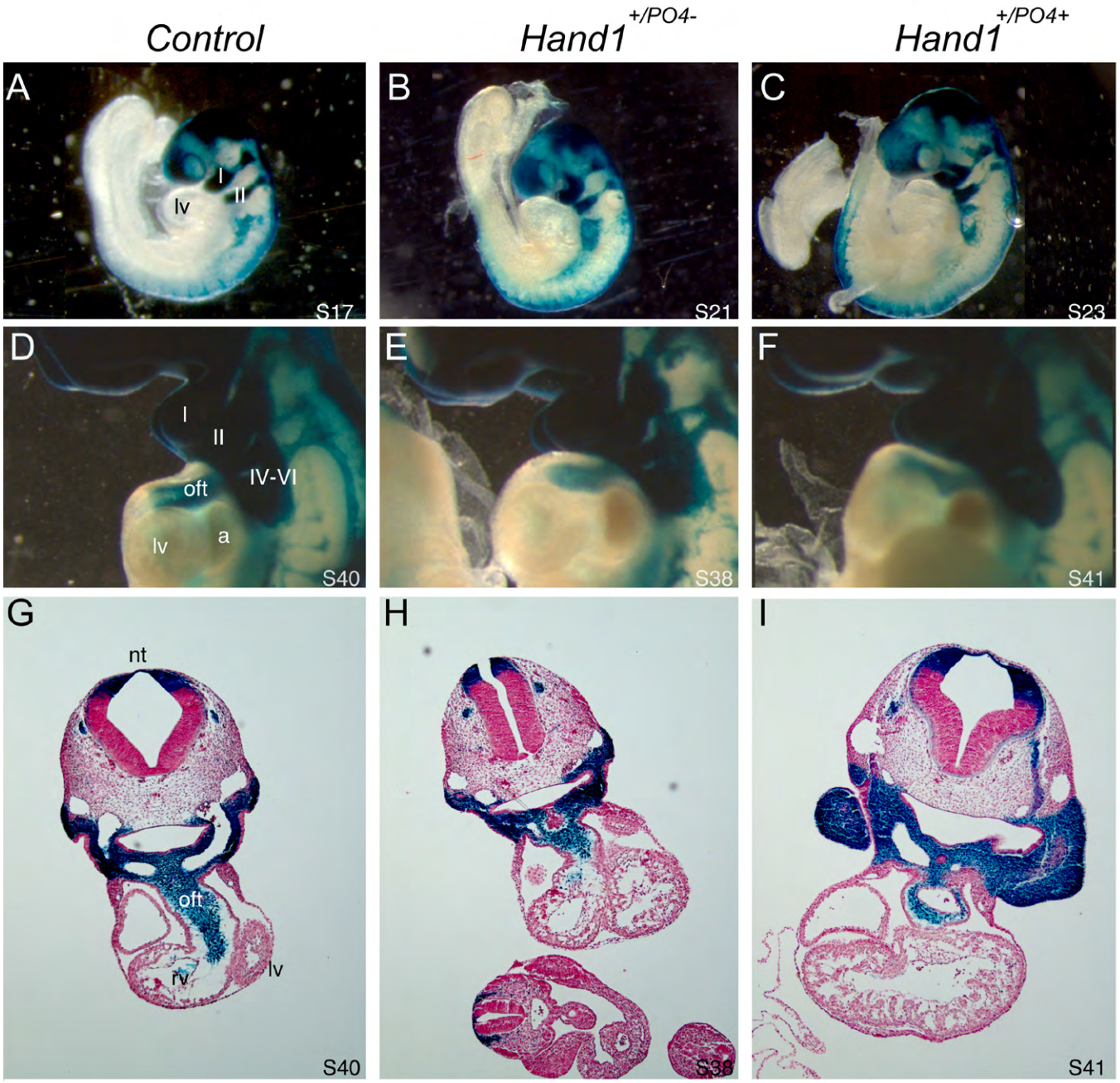

Supplementary Figure 3: Analysis of NCC migration in Control, *Hand1*$^{+/PO4-}$, and *Hand1*$^{+/PO4+}$ embryos on the *R26R* background. Lateral views of E9.5 day Control (A), *Hand1*$^{+/PO4-}$ (B), and *Hand1*$^{+/PO4+}$ (C), show no significant changes in the *Wnt1-Cre* activation of β-galactosidase within the NCC. Lateral views at E11.5, robust and indistinguishable numbers of reporter-marked NCC are observed in all of the pharyngeal arches and cardiac outflow tract (oft) of both Control and phospho-mutant embryos. (G-I) show transverse sections confirming the presence of β-galactosidase-marked NCC within the OFT. Pharyngeal arches are indicated by roman numerals; left ventricle (lv), atria (a). Somite numbers are indicated in the lower right hand corners of each panel. n≥4 for each genotype.

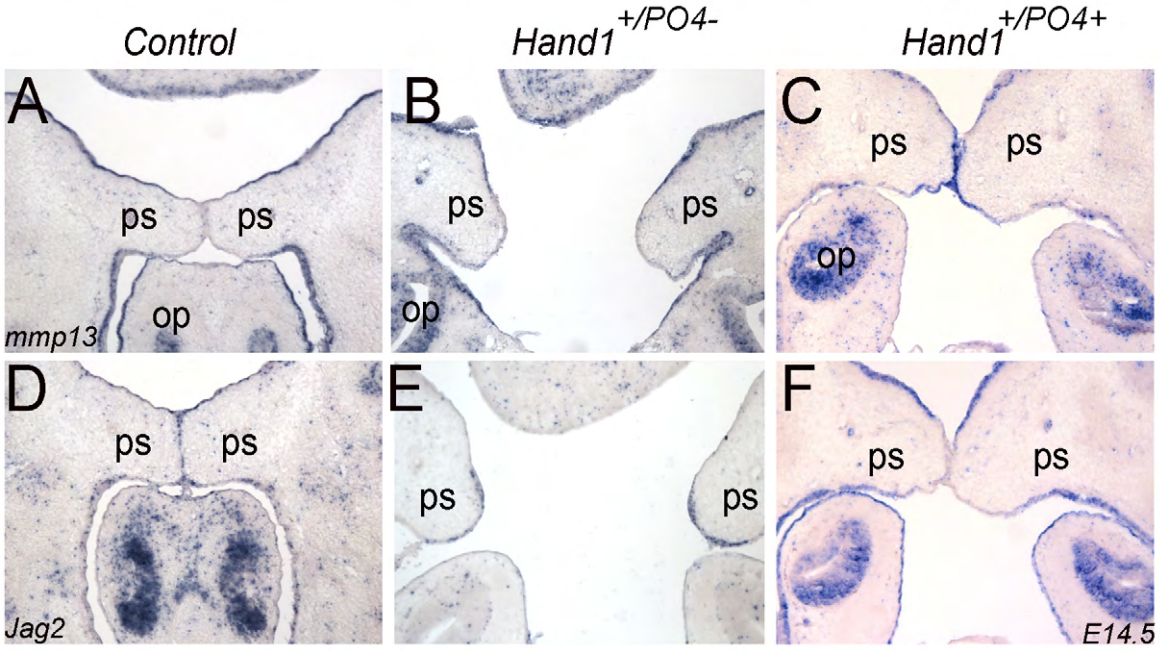

Supplementary Figure 4: E14.5 section *in situ* hybridization analysis of the fusion markers Mmp13 and Jagged 2 in *control* (A and D), *Hand1*$^{+/PO4-}$ (B and E), *and Hand1*$^{+/PO4+}$ (C and F) embryos. *Control* sections show the initiation of fusion of the palatal shelves (ps) just dorsal to the olfactory pits (op). *Mmp13* expression marks the surrounding epithelium of the palatal shelves as well as the cells surrounding the nasal septum. In Hand1 phospho-mutant embryos Mmp13 expression patterns are not significantly different. Similarly *Jagged*2 expression mirrors that of Mmp13 in both control (D) and phospho mutants (E and F). n≥4 for each genotype.

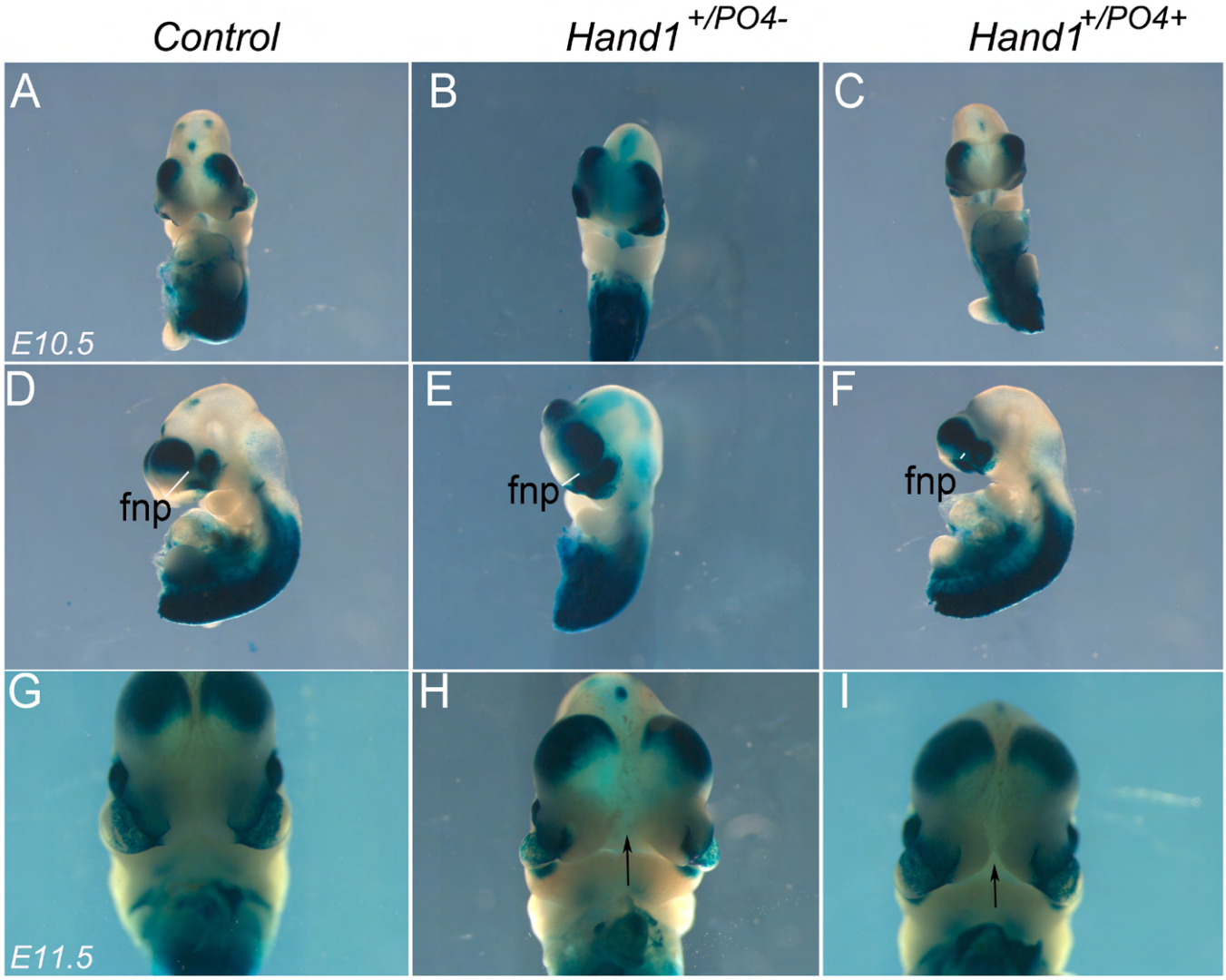

Supplementary Figure 5: β-Galactosidase activity showing expression of the Retinoic Acid Reporter Element (RARE) lacZ reporter in *Control* (A, D, G), activated *Hand1*$^{+/PO4-}$ (B, E, H), and *Hand1*$^{+/PO4+}$ (C, F, I) backgrounds. E10.5 Phospho mutants show a reduction in frontal nasal process (fnp) tissue; however the RA signaling underlining the tissue is largely unaffected. Similarly at E11.5 no significant difference in RA-induced β- Galactosidase staining is evident in between control (G) Hand1 phospho mutants (H and I). Black arrows point to the forming mid-face cleft. n≥4 for each genotype.

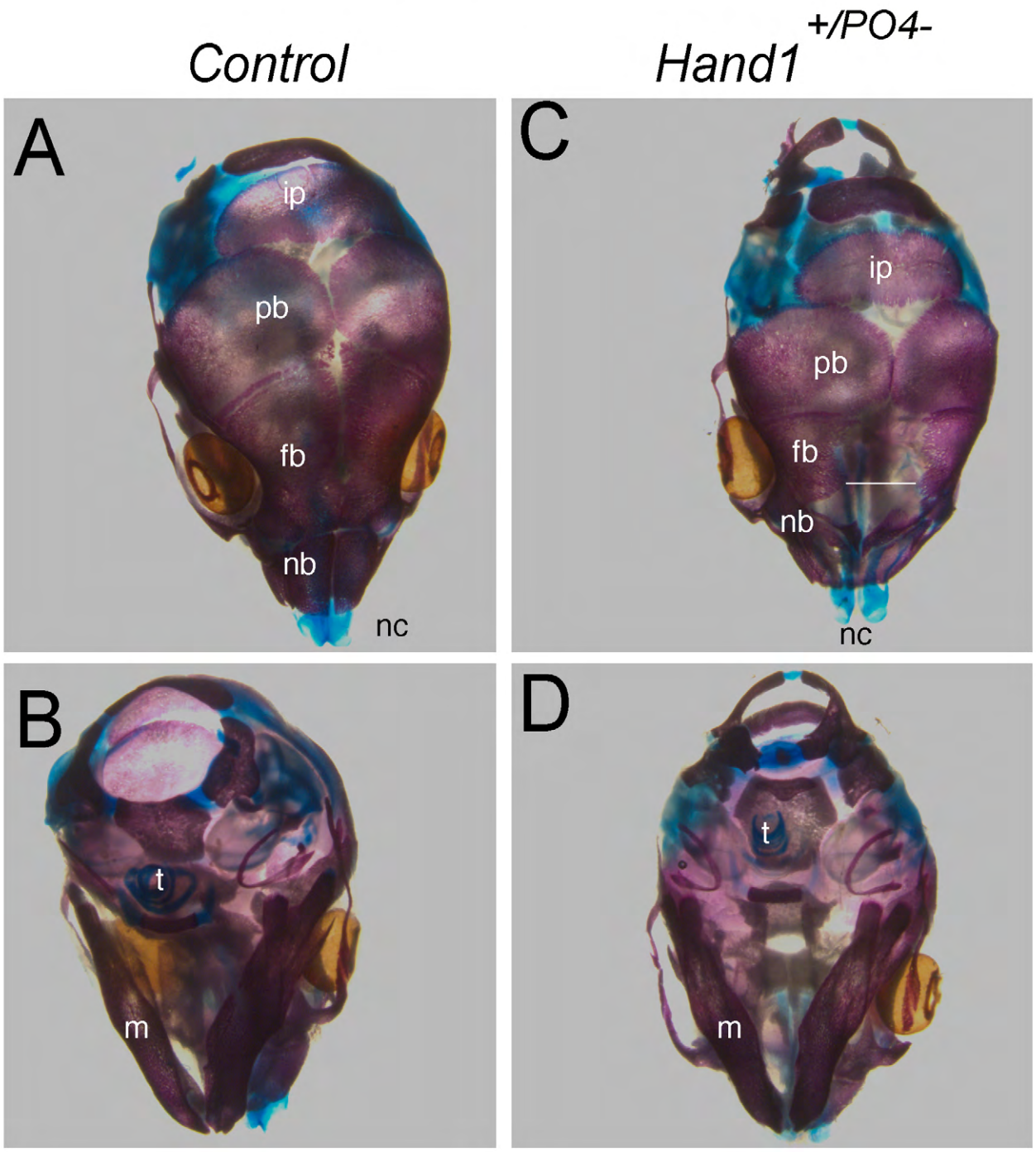

Supplementary Figure 6: Activation of Hand1 phospho-mutant expression using *P0-Cre* reduces the severity of cranio-facial phenotypes. The *P0-Cre* transgene is expressed in migrating NCCs becoming active a day later than the *Wnt1-Cre* transgene. (Yamauchi et al., 1999) Comparison of E18.5 day *control* (A and B) and activated *Hand1*$^{+/PO4-}$ (C and D) heads show that fusion of the nasal capsule (nc) is nearly complete though still not phenotypically normal. Nasal bones (nb) and frontal bones (fb) are reduced in size and the white bar marks the gap between the left and right frontal bonds, which is absent in *controls*. Ventral views (B and D) reveal that palate formation in the *Hand1*$^{+/PO4-}$ embryo is vastly improved. As the *P0-Cre* transgene is expressed within the pharyngeal arch NCC mesenchyme nearly concurrently with *Hand1*, the obvious temporal delay of deletion of the Stop-flox cassette supports the data in Figure 2 suggesting that the deleterious effects of Hand1 phospho-mutant expression are immediate upon its initial activation. Trachea (t) is labeled in ventral views. n≥4 for each genotype.

Supplementary Table 1. Skeletal lengths and area measurements from Micro-CT scanning.

Skeletal Region	WT	A+	A-	D+	D-
Mandible Area (mm^2) ± 0.194*¥	5.698 ± 0.158¥	3.170 ± 0.158*	5.088 ± 0.194*¥	4.718 ± 0.158*¥	4.721
Mandible Length (mm) ± 0.073*¥	5.021 ± 0.059¥	3.442 ± 0.059*	4.331 ± 0.073*¥	4.108 ± 0.059*¥	4.168
Tympanic Length (mm) ± 0.139*¥	2.014 ± 0.114¥	0.609 ± 0.114*	1.996 ± 0.139¥	1.760 ± 0.114¥	1.507
Premaxilla Area (mm^2) ± 0.115*	1.546 ± 0.094	0.690 ± 0.094*	0.862 ± 0.115*¥	0.958 ± 0.094*	0.940
Premaxilla Length (mm) ± 0.095*¥	1.970 ± 0.078¥	1.141 ± 0.078*	1.302 ± 0.095*	1.545 ± 0.078*¥	1.552
Zygomatic arch Length (mm) ± 0.102*¥	4.329 ± 0.102¥	1.843 ± 0.102*	3.573 ± 0.125*¥	3.412 ± 0.102*¥	3.202
Squamous Area (mm^2) ± 0.030*¥	0.638 ± 0.030¥	0.021 ± 0.030*	0.280 ± 0.037*¥	0.198 ± 0.037*¥	0.235
Palate Left Area (mm^2) ± 0.089¥	0.952 ± 0.072¥	0.134 ± 0.072*	0.650 ± 0.089*¥	0.552 ± 0.072*¥	0.727
Palate Right Area (mm^2) ± 0.061¥	0.934 ± 0.050¥	0.188 ± 0.050*	0.576 ± 0.061*¥	0.647 ± 0.050*¥	0.797
Basisphenoid Area (mm^2) ± 0.078*	1.220 ± 0.064	0.375 ± 0.064*	0.626 ± 0.078*¥	0.583 ± 0.476*¥	0.476
Presphenoid Area (mm^2) ± 0.133	0.816 ± 0.108	0.627 ± 0.108	1.478 ± 0.133*¥	1.168 ± 0.108*¥	0.952
Pterygoid Left Area (mm^2) ± 0.022*	0.194 ± 0.018¥	0.024 ± 0.018*	0.109 ± 0.022*	0.149 ± 0.018*	0.191
Pterygoid Right Area (mm^2) ± 0.032¥	0.191 ± 0.027¥	0.017 ± 0.027*	0.097 ± 0.032	0.136 ± 0.027¥	0.204
Incisor Distance (mm) ± 0.321¥	0.184 ± 0.262¥	2.465 ± 0.262*	1.892 ± 0.321*	0.873 ± 0.262¥	0.849
Palate Distance (mm) ± 0.208¥	0.866 ± 0.170¥	2.113 ± 0.170*	1.969 ± 0.208*	1.511 ± 0.170*¥	1.083

*Significantly different from WT; ¥significantly different from A+